Supporting Information

Constructing donor-acceptor molecules as blue emitters with nonsymmetrical connection for organic emitting diodes

Jayaraman Jayabharathi*, Jagathratchagan Anudeebhana, Venugopal Thanikachalam, Sekar Sivaraj, Annadurai Prabhakaran

Department of Chemistry, Materials science lab, Annamalai University, Annamalainagar 608 002, Tamilnadu, India

.

Address for correspondence

•Dr. J. Jayabharathi

Professor of Chemistry
Department of Chemistry
Materials science lab
Annamalai University
Annamalai nagar 608 002
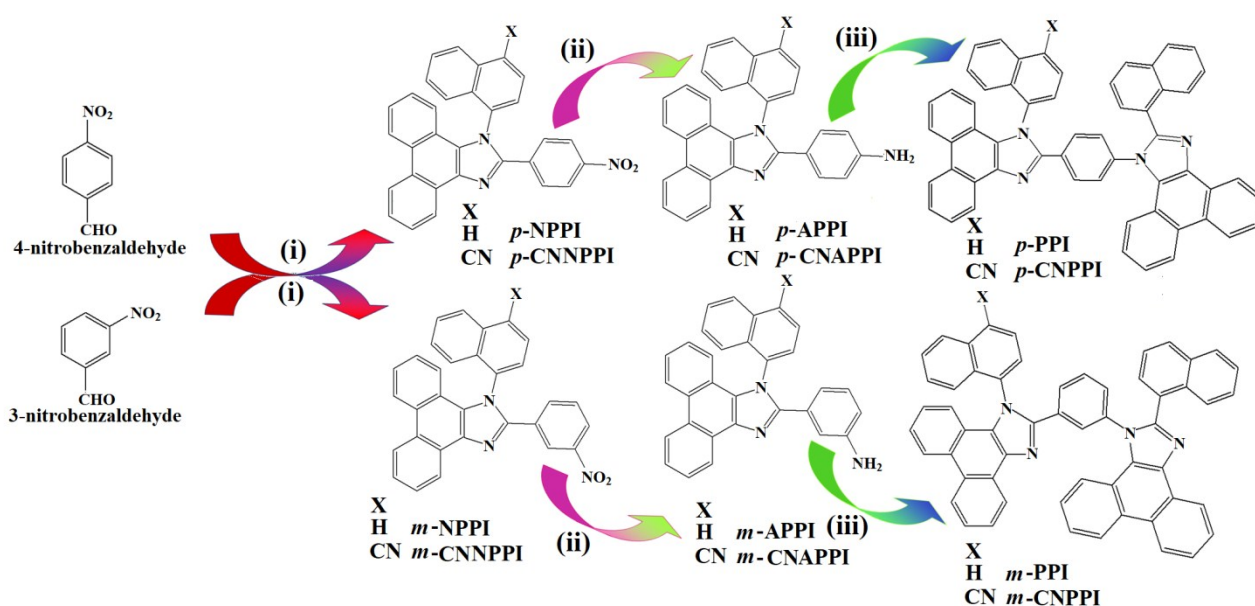Tamilnadu, India.
E-mail: jtchalam2005@yahoo.co.in

Contents

SI–I: Scheme S1. Synthetic route of *p*-PPI, *p*-CNPPI, *m*-PPI and *m*-CNPPI.

(i) **phenanthrenequinone, naphthalene-1-amine, ammonium acetate, glacial acetic acid;**

(ii) **10% Pd/C, 80% hydrazine hydrate, ethanol, reflux;**

(iii) **phenanthrenequinone, 1-naphthaldehyde, ammonium acetate, glacial acetic acid.**

I.1. 1-(naphthalen-1-yl)-2-(4-nitrophenyl)-1*H*-phenanthro [9,10-d]imidazole (*p*-NPPI)

A mixture of phenanthrene-9,10-dione (2.08 g, 10 mmol), 4-nitrobenzaldehyde (1.51 g, 10 mmol), 1-naphthylamine (4.65 g, 50 mmol) with ammonium acetate (3.08 g, 40 mmol) in acetic acid (25 ml) was refluxed at 120° C for 12 h under nitrogen atmosphere and poured into methanol. The separated yellowish green crude was purified by column with hexane: ethyl acetate as the eluent (Figure S1). ^{1}H NMR (400 MHz, CDCl$_3$): 7.3 (d, 4H), 7.7- 7.74 (m, 5H), 7.82 - 7.88 (m, 4H), 8.12 (d, 2H), 8.25 (d, 2H), 8.93 (d, 2H). ^{13}C- NMR (CDCl$_3$, 100 MHz,): 121.6, 122.4, 124.1,

126.3, 126.6, 127.2, 127.6, 127.8, 128.3, 128.4, 130.7, 131.5, 132.2, 134.6, 136.8, 148.4, 149.4. MS: m/z. 465.22 [M+]; Calcd. 465.15.

I.2. 4-(1-(naphthalen-1-yl)-1*H*-phenanthro[9,10-d]imidazol-2-yl)benzenamine (*p*-APPI)

A mixture of 1-(naphthalen-1-yl)-2-(4-nitrophenyl)-1H-phenanthro[9,10-d]imidazole (NPPI) (4.15 g,10 mmol) and 10 % Pd/C (250 mg) in 25 ml ethanol was refluxed under stirring and 80 % hydrazine hydrate (15 ml) was added slowly for 30 min and the stirring was continued for 12 h, the reaction mixture was neutralized with aqueous HCl. The white product was recrystallized from ethanol: water mixture(Figure S2). Yield: 65%. 1H NMR (400 MHz, CDCl$_3$) 4.0 (d, 2H), 6.52 (d, 2H), 7.23 (d, 2H), 7.3 (t, 4H), 7.7 (d, 2H), 7.82-7.88 (m, 4H), 8.12 (d, 2H), 8.93 (d, 2H). ^{13}C NMR (CDCl$_3$, 100 MHz,): 116.8, 120.7, 122.4, 124.1, 126.3, 126.6, 127.2, 127.6, 127.8, 128.3, 130.7, 131.5, 132.2, 134.6, 148.4, 149.4. MS: m/z. 435.22 [M+]; Calcd. 435.17.

I.3. 2-(naphthalen-1-yl)-1-(4-(1-(naphthalen-1-yl)-1*H*-phenanthro[9,10-d]imidazol-2-yl) phenyl)-1-*H*-phenanthro[9,10-d]imidazole (*p*-PPI)

A mixture of phenanthrenequinone (0.416 g, 2 mmol), 1-naphthaldehyde (0.698 g, 2 mmol), (4-(1-(naphthalen-1-yl)-1*H*-phenanthro[9,10-d]imidazol-2-yl)benzenamine (APPI) (1.16 g, 3 mmol), ammonium acetate (1.54 g, 20 mmol) and glacial acetic acid (25 ml) was refluxed at 120° C for 12 h under nitrogen atmosphere [25] and poured into methanol. The separated white solid was subjected to water washings and purified by column using CH$_2$Cl$_2$ as the eluent(Figure S3). Yield: 52%.1H NMR (400 MHz, CDCl$_3$, ppm): 7.3 (d, 3H), 7.32-7.38 (m, 6H), 7.5-7.54 (m, 3H), 7.63-7.70 (m, 6H), 7.82 (m, 4H), 7.88 (m, 4H), 8.12 (d, 4H), 8.93 (d, 4H). ^{13}C NMR (CDCl$_3$, 100 MHz): (122.4, 122.9, 124.1, 124.7, 126.3, 126.6, 126.8, 127.6, 127.8, 128.3, 128.4, 130.2, 130.7, 131.5, 132.2, 132.7, 134.2, 134.6, 136.0, 137.4, 149.4. MALDI-TOF MS: m/z. 761.50 [M]+ (calcd: 762.28). Anal.calcd (%) for C$_{56}$H$_{34}$N$_4$: C, 88.16; H, 4.49; N, 7.34. Found: C, 88.14; H, 4.80; N, 7.35.

I.4. 4-(2-(4-nitrophenyl)-1*H*-phenanthro[9,10-d]imidazol-1-yl)naphthalene-1-carbonitrile (*p*-CNNPPI)

The *p*-CNNPPI was synthesized using 4-aminonaphthalene-1-carbonitrile and the methodology is similar to that of *p*-NPPI(Figure S4). ^{1}H NMR (400 MHz, CDCl$_3$) 7.4 (d, 1H), 7.5 - 7.6 (m, 2H), 7.74 - 7.88 (m, 8H), 8.12 -8.25 (m, 5H), 8.93 (d, 2H). ^{13}C NMR (CDCl$_3$, 100 MHz): 109.5, 115.8, 116.8, 121.6, 121.7, 122.4, 123.8, 126.5, 126.6, 127.5, 127.6, 128.3, 128.4, 128.5, 131.5, 132.7, 133.4, 136.0, 136.8, 148.4, 149.4. MS: m/z. 490.19 [M$^+$]; Calcd. 490.14.

I.5. 4-(2-(4-aminophenyl)-1*H*-phenanthro[9,10-d]imidazol-1-yl)naphthalene-1-carbonitrile (*p*-CNAPPI)

Compound *p*-CNAPPI was synthesized using *p*-CNNPPI and the methodology is similar to that of *p*-APPI(Figure S5). ^{1}H NMR (400 MHz, CDCl$_3$) 4.0 (d, 2H), 6.52 (d, 2H), 7.23 (t, 2H), 7.4 (d, 1H), 7.5-7.6 (m, 2H), 7.8 -7.88 (m, 6H), 8.12 -8.2 (m, 3H), 8.93 (d, 2H). ^{13}C NMR (CDCl$_3$, 100 MHz): 109.5, 115.8, 116.8, 120.7, 121.7, 122.4, 123.8, 126.5, 126.6, 127.5, 127.6, 128.3, 128.5, 131.5, 132.7, 133.4, 136.0, 148.4, 149.4. MS: m/z. 460.28 [M$^+$]; Calcd. 460.17.

I.5. 4-(2-(4-(2-(naphthalen-1-yl)-1*H*-phenanthro[9,10-d]imidazol-1-yl)phenyl)-1*H*-phenanthro[9,10-d]imidazol-1-yl)naphthalene -1-carbonitrile (*p*-CNPPI)

The *p*-CNPPI was synthesized using *p*-CNAPPI and the methodology is similar to that of *p*-PPI(Figure S6). Yield: 70%, ^{1}H NMR (400 MHz, CDCl$_3$, ppm): (7.3 (d, 2H), 7.32 -7.54 (m, 8H), 7.6 - 7.67 (m, 4H), 7.8 -7.82 (m, 7H), 7.88 (m, 4H), 8.12 (m, 4H), 8.93 (d, 2H). ^{13}C NMR (CDCl$_3$, 100 MHz): 109.5, 115.8, 121.7, 122.4, 122.9, 123.8, 124.7, 126.3, 126.5, 126.6, 127.5, 127.6, 128.3, 128.4, 128.5, 130.2, 131.5, 132.7, 133.4, 134.2, 136.0, 137.4, 149.4. MALDI-TOF MS: m/z. 787.38 [M]$^+$ (calcd: 787.27). Anal. calcd (%) for C$_{57}$H$_{33}$N$_5$: C, 86.89; H, 4.22; N, 8.89. Found: C, 86.66; H, 4.32; N, 8.71.

I.6. 4-(2-(3-nitrophenyl)-1*H*-phenanthro[9,10-d]imidazol-1-yl)naphthalene-1-carbonitrile (*m*-NPPI)

The synthetic methodology is similar to that of *p*-NPPI by using *m*-nitrobenzaldehyde instead of *p*- nitrobenzaldehyde. Yield 68% (Figure S7). ^{1}H NMR (400 MHz, CDCl$_3$, ppm): 7.3 (d, 4H), 7.58-7.7 (m, 4H), 7.82 -7.88 (m, 10 H), 8.12 -8.15 (t, 3H), 8.41 (s, 1H), 8.93 (d, 2H).^{13}C NMR

(CDCl$_3$, 100 MHz): 121.1, 122.1, 122.4, 124.1, 126.3, 126.6, 127.6, 127.8, 128.3, 130.2, 130.7, 131.5, 131.6, 132.2, 133.6, 134.6, 148.0, 149.4. MALDI-TOF MS: m/z. 465.22 [M]$^+$ (calcd: 465.15). Anal. calcd (%) for C$_{31}$H$_{19}$N$_3$O$_2$: C, 79.99; H, 4.11; N, 9.03. Found: C, 80.11; H, 4.32; N, 9.25.

I.7. 3-(1-(naphthalen-1-yl)-1*H*-phenanthro[9,10-d]imidazol-2-yl)benzenamine (*m*-APPI)

Yield 70% (Figure S8). ^{1}H NMR (400 MHz, CDCl$_3$, ppm): 4.0 (d, 2H), 6.42 (d, 1H), 6.68 (d, 1H), 6.84 - 7.3 (m, 6H), 7.7 (d, 3H), 7.82 -7.88 (m, 4H), 8.12 (d, 2H), 8.93 (d, 2H). ^{13}C NMR (CDCl$_3$, 100 MHz): 114.2, 116.3, 117.5, 122.4, 124.1, 126.3, 126.6, 127.2, 127.6, 127.8, 128.3, 130.1, 130.7, 131.5, 132.2, 134.6, 148.9, 149.4. MALDI-TOF MS: m/z. 435.12 [M]$^+$ (calcd: 435.17).

I.8. 2-(naphthalen-1-yl)-1-(3-(1-(naphthalen-1-yl)-1*H*-phenanthro[9,10-d]imidazol-2-yl)phenyl)-1*H*-phenanthro[9,10-d]imidazole (*m*-PPI)

Yield 70% (Figure S9). ^{1}H NMR (400 MHz, CDCl$_3$, ppm): 7.2 (d, 1H), 7.3-7.32 (m, 6H), 7.38 -7.54 (m, 4H), 7.67-7.7 (m, 5H), 7.82-7.88 (m, 8H), 8.12 (d, 4H), 8.93 (d, 4H). ^{13}C NMR (CDCl$_3$, 100 MHz): 22.6, 119.5, 122.4, 124.1, 124.7, 126.3, 126.6, 126.8, 127.6, 127.8, 128.3, 130.2, 130.7, 131.5, 131.6, 132.2, 132.7, 134.2, 134.6, 136.0, 137.9, 149.4. MALDI-TOF MS: m/z. 762.32 [M]$^+$ (calcd: 762.28). Anal. calcd (%) for C$_{56}$H$_{34}$N$_4$: C, 88.16; H, 4.49; N, 7.34. Found: C, 88.11; H, 4.56; N, 7.22.

I.9. 4-(2-(3-nitrophenyl)-1*H*-phenanthro[9,10-d]imidazol-1-yl)naphthalene-1-carbonitrile(*m*-CNNPPI)

Yield 70% (Figure S10). ^{1}H NMR (400 MHz, CDCl$_3$, ppm): 7.4 (d, 1H), 7.5 -7.6 (m, 3H), 7.8 -7.87 (m, 7H), 8.15-8.2 (m, 4H), 8.41 (s, 1H), 8.93 (d, 2H). ^{13}C NMR (CDCl3, 100 MHz): 109.5, 115.8, 121.1, 121.7, 122.1, 122.4, 123.8, 126.5, 126.6, 127.5, 127.6, 128.3, 128.5, 130.2, 131.5, 131.6, 132.7, 133.4, 133.6, 136.0, 148.0, 149.4. MALDI-TOF MS: m/z. 490.21 [M]$^+$ (calcd: 490.14).

I.10. 4-(2-(3-aminophenyl)-1*H*-phenanthro[9,10-d]imidazol-1-yl)naphthalene-1-carbonitrile (*m*-CNAPPI)

Yield 70%(Figure S11). ^{1}H NMR (400 MHz, CDCl$_3$, ppm): 4.0 (d, 2H), 6.42 (d, 1H), 6.68

(d, 1H), 6.84 (t, 1H), 7.07 (m, 1H), 7.4 (d, 1H), 7.5 -8.12 (m, 8H), 8.12 -8.2 (m, 3H), 8.93 (d, 2H).
^{13}C NMR (CDCl$_3$, 100 MHz): 109.5, 114.2, 115.8, 116.3, 117.5, 121.7, 122.4, 123.8, 126.5, 126.6, 127.5, 127.6, 128.3, 128.5, 130.1, 131.5, 132.7, 133.4, 136.0, 148.9, 149.4. MALDI-TOF MS: m/z. 460.28 [M]$^+$ (calcd: 460.17).

I.11. 4-(2-(3-(2-(naphthalen-1-yl)-1*H*-phenanthro[9,10-d]imidazol-1-yl)phenyl)-1*H*-phenanthro[9,10-d]imidazol-1-yl)naphthalene-1-carbonitrile(*m*-CNPPI)

Yield 70%(Figure S12). ^{1}H NMR (400 MHz, CDCl$_3$, ppm): 7.2 (d, 1H), 7.3-7.32 (m, 3H), 7.38-7.5 (m, 6H), 7.54-7.67 (m, 5H), 7.80-7.88 (m, 10H), 8.12-8.2 (m, 5H), 8.93 (d, 4H). ^{13}C NMR (100 MHz, CDCl$_3$): (109.5, 115.8, 119.5, 121.7, 122.4, 123.8, 124.7, 126.3, 126.5, 126.6, 126.8, 127.6, 128.3, 128.5, 130.2, 131.5, 131.6, 132.7, 133.4, 134.2, 136.0, 137.9, 149.4. MALDI-TOF MS: m/z. 787.10 [M]$^+$ (calcd: 787.27). Anal. calcd (%) for C$_{57}$H$_{33}$N$_5$: C, 86.89; H, 4.22; N, 8.89. Found: C, 86.72; H, 4.41; N, 8.94.

Figure S1. H^1 and C^{13} NMR spectra of *p*-NPPI
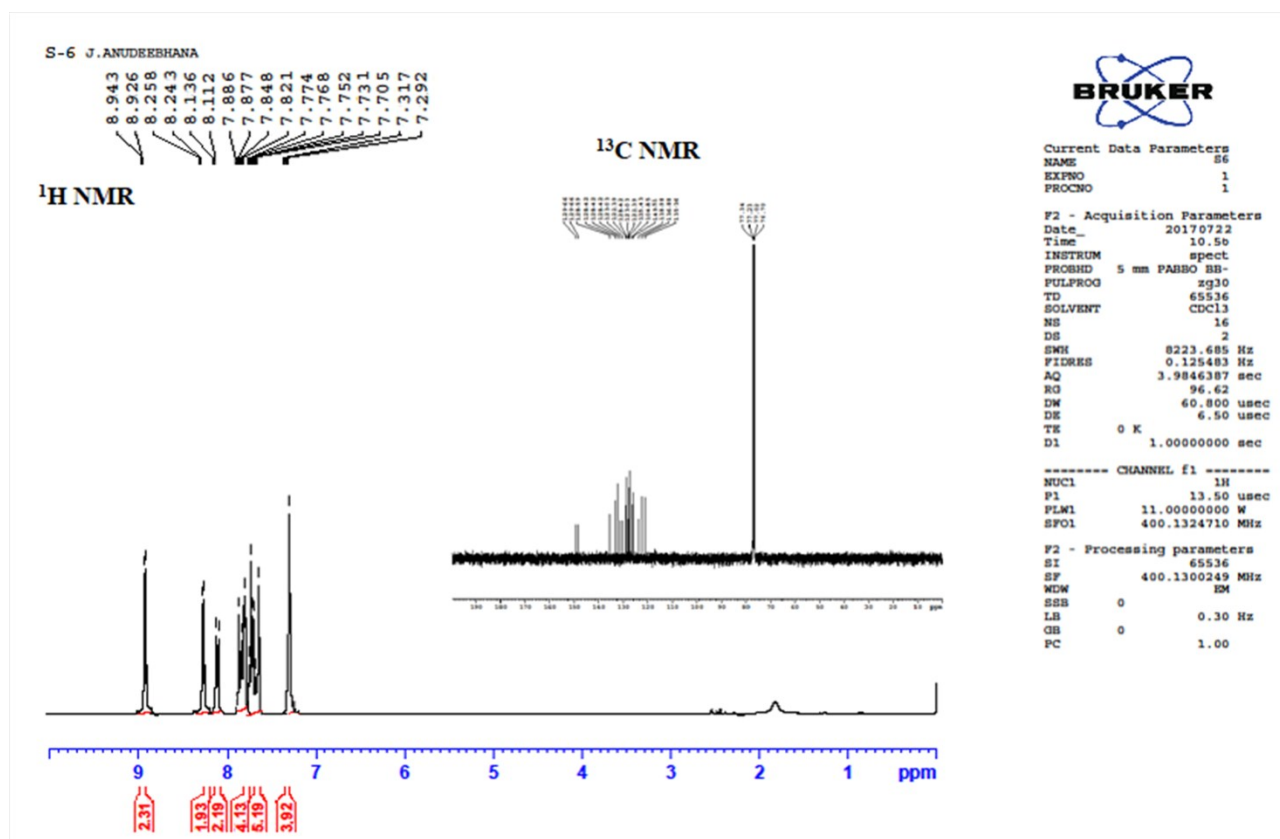
Figure S2. H¹ and C¹³ NMR spectra of *p*-APPI
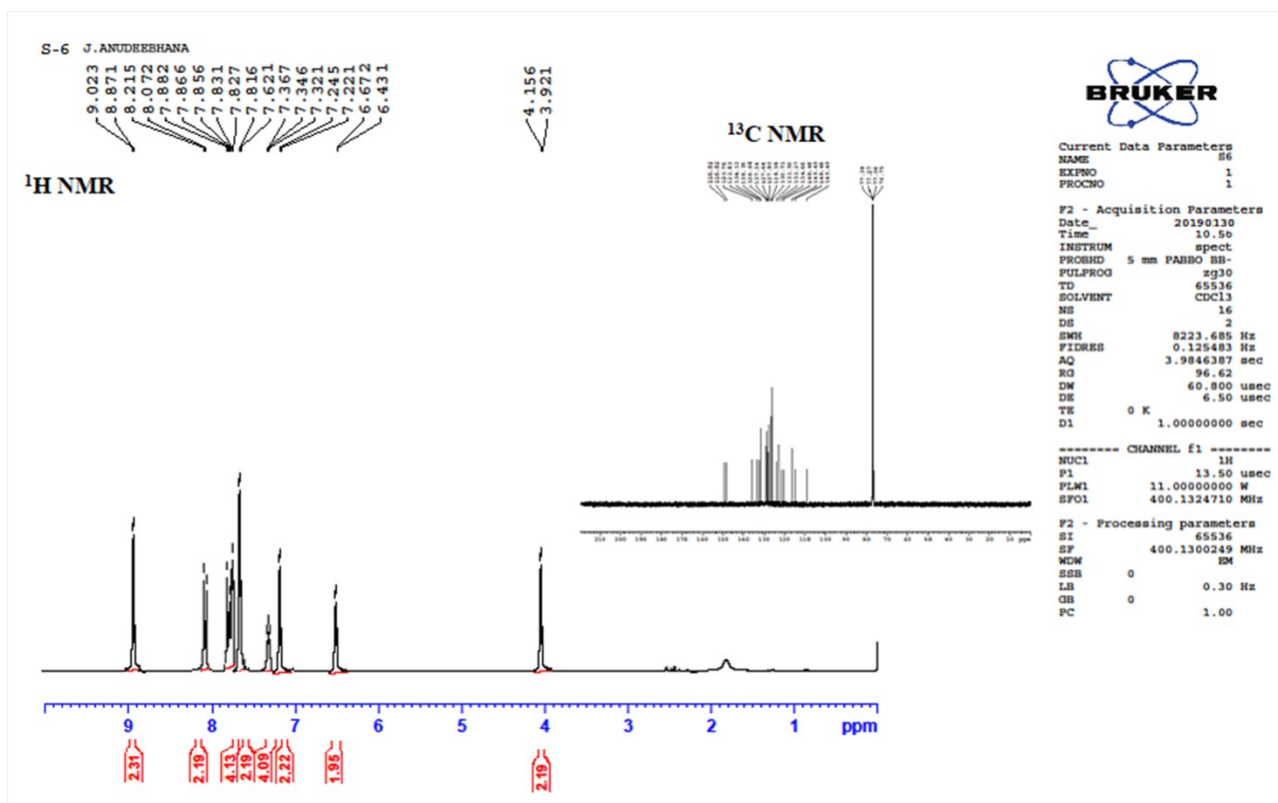
Figure S3. H¹ and C¹³ NMR spectra of *p*-PPI
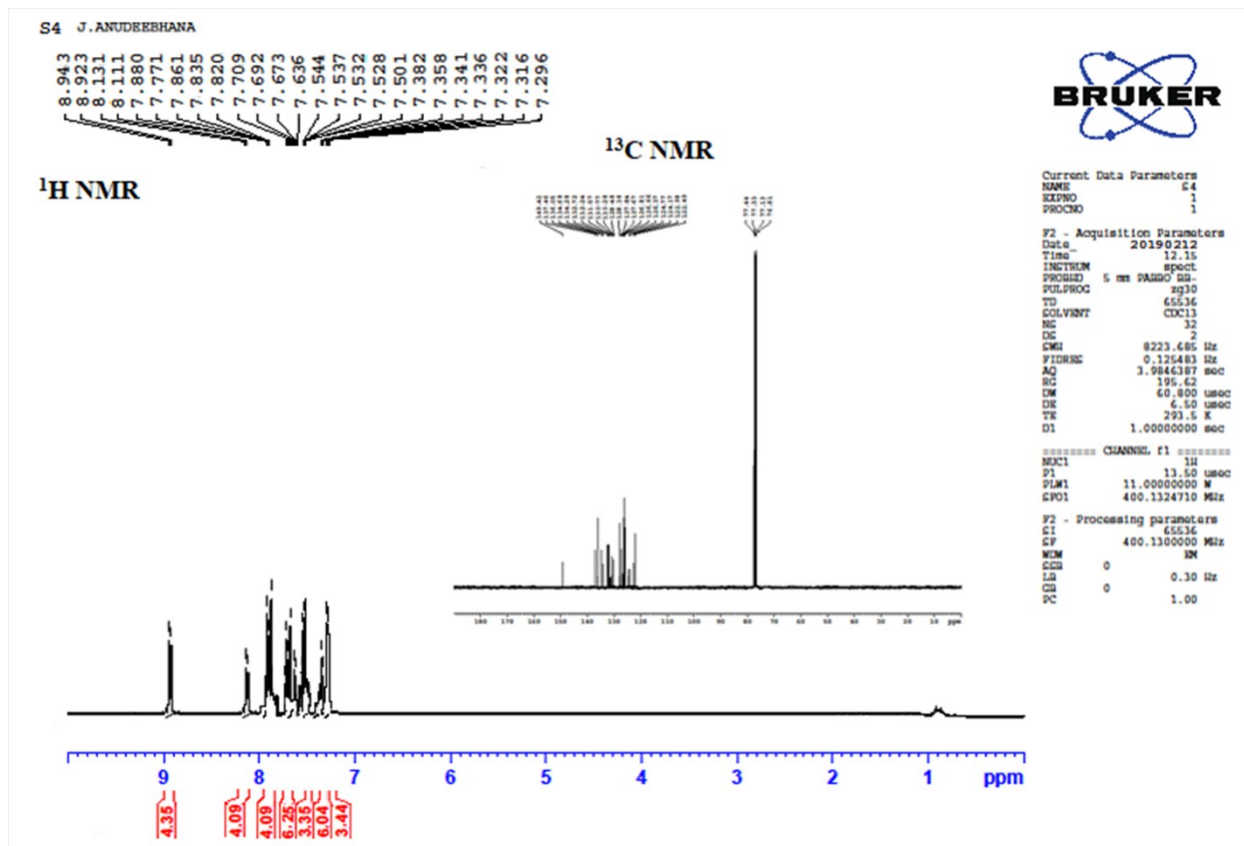
Figure S4. H¹ and C¹³ NMR spectra of *p*-CNNPPI
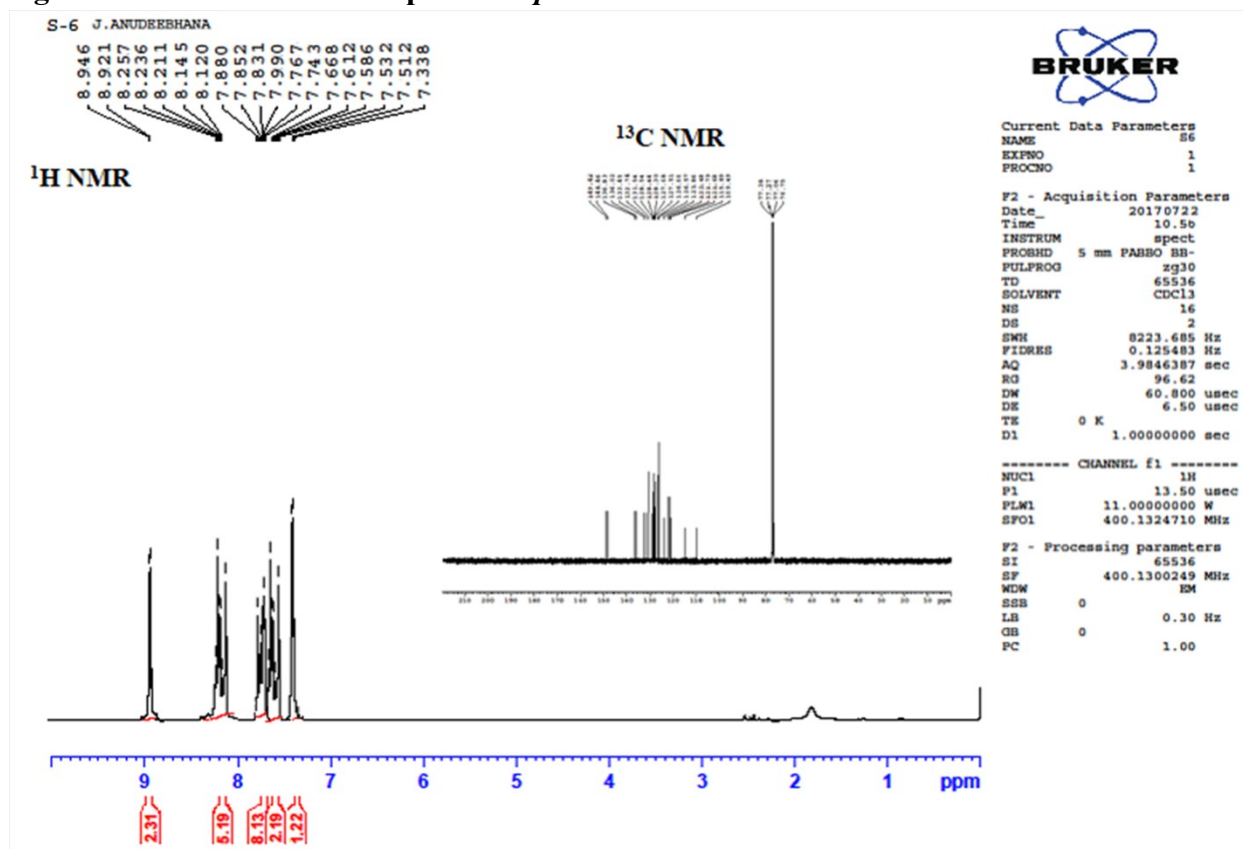
Figure S5. H¹ and C¹³ NMR spectra of *p*-CNAPPI
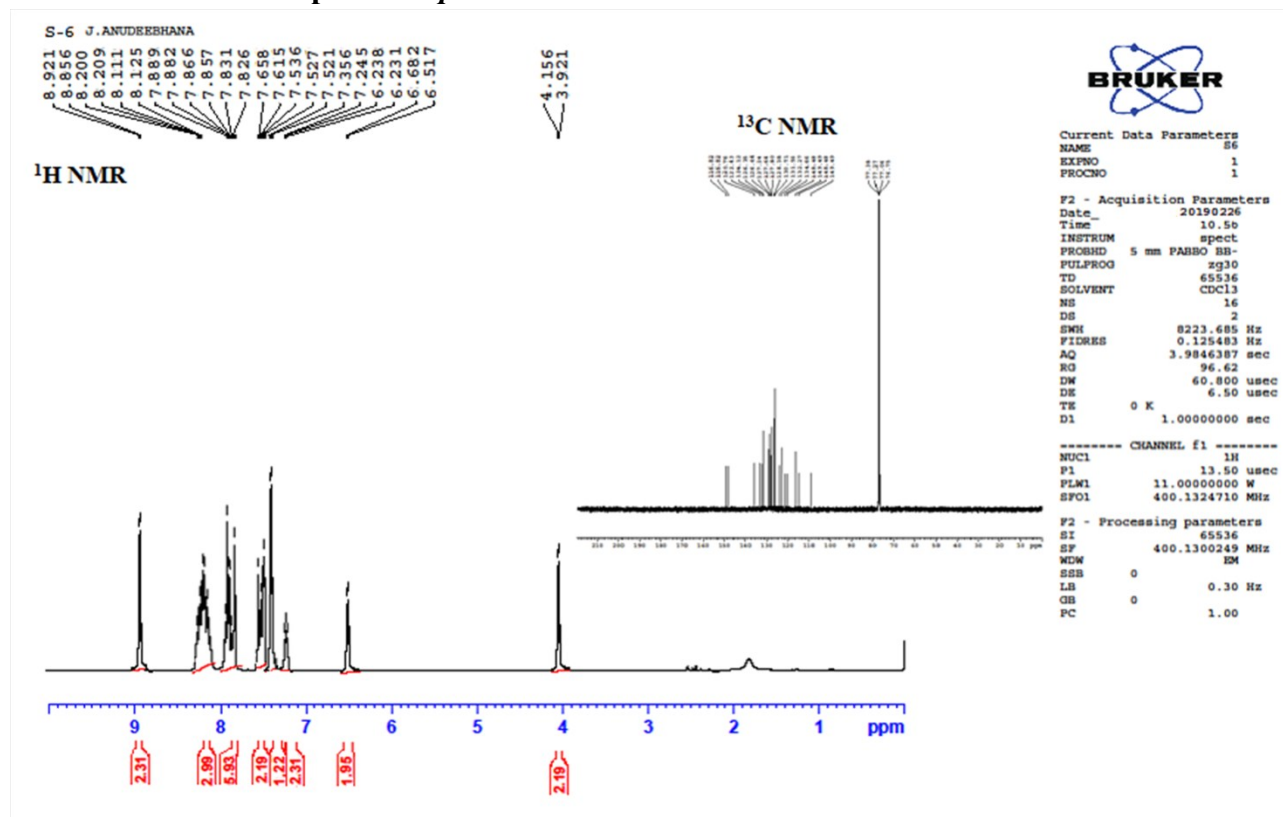
Figure S6. H^1 and C^{13} NMR spectra of *p*-CNPPI
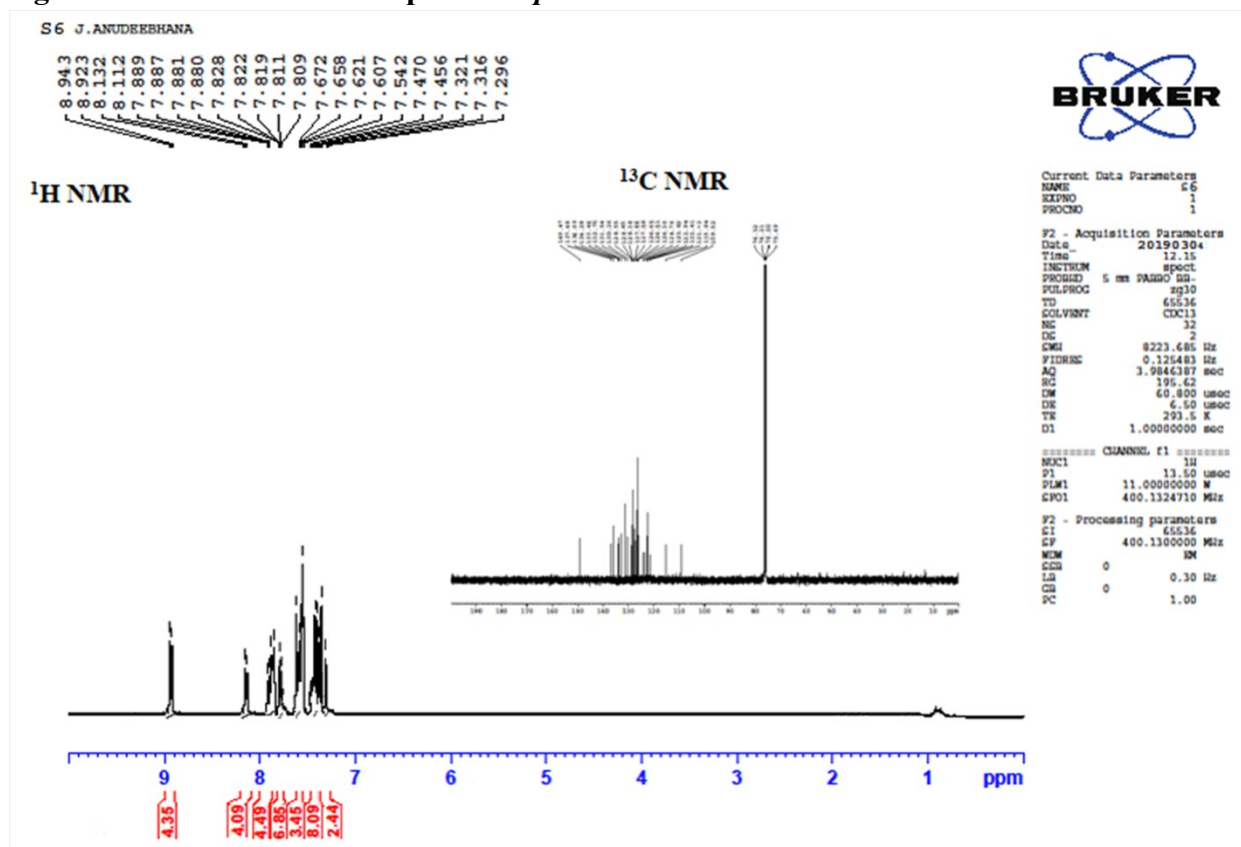
Figure S7. H^1 and C^{13} NMR spectra of *m*-NPPI
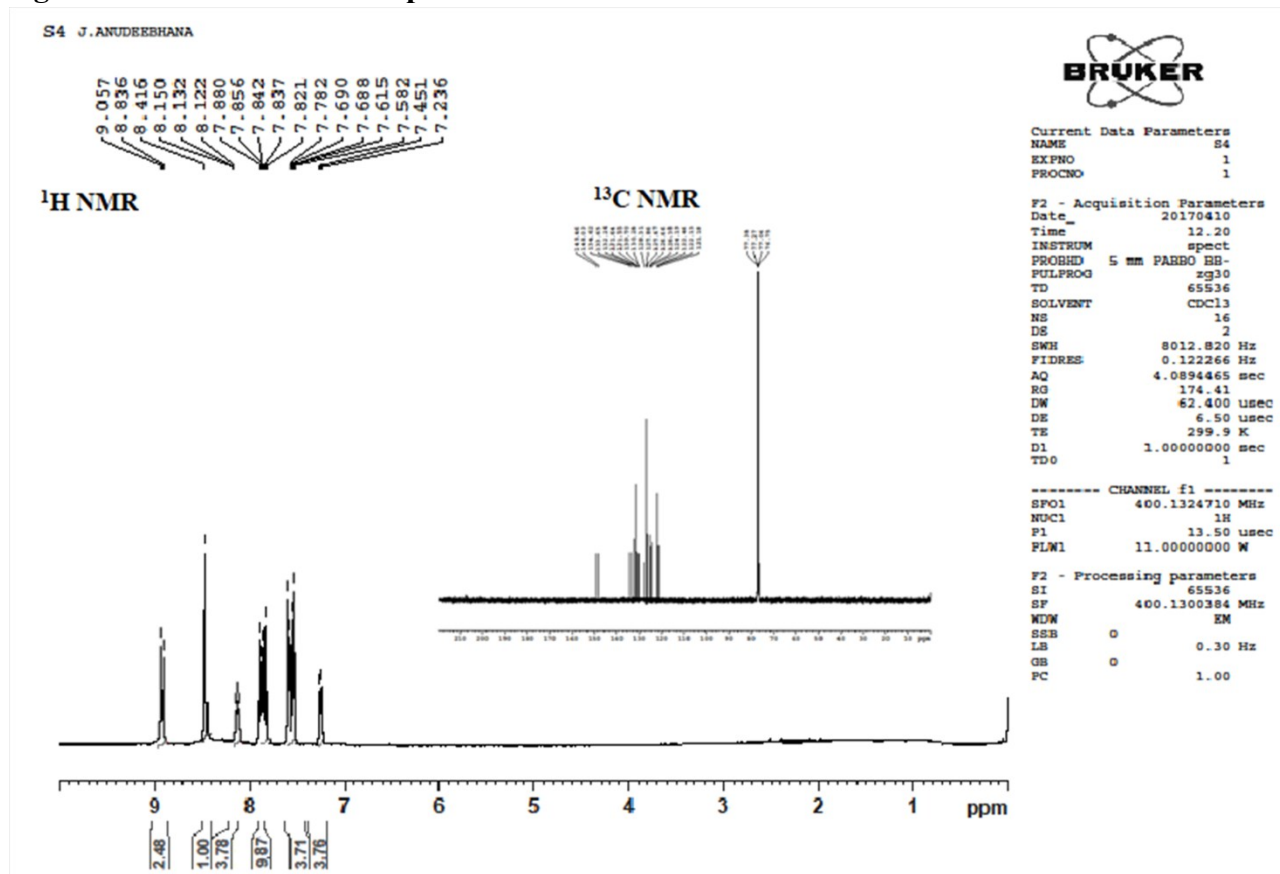
Figure S8. H^1 and C^{13} NMR spectra of *m*-APPI
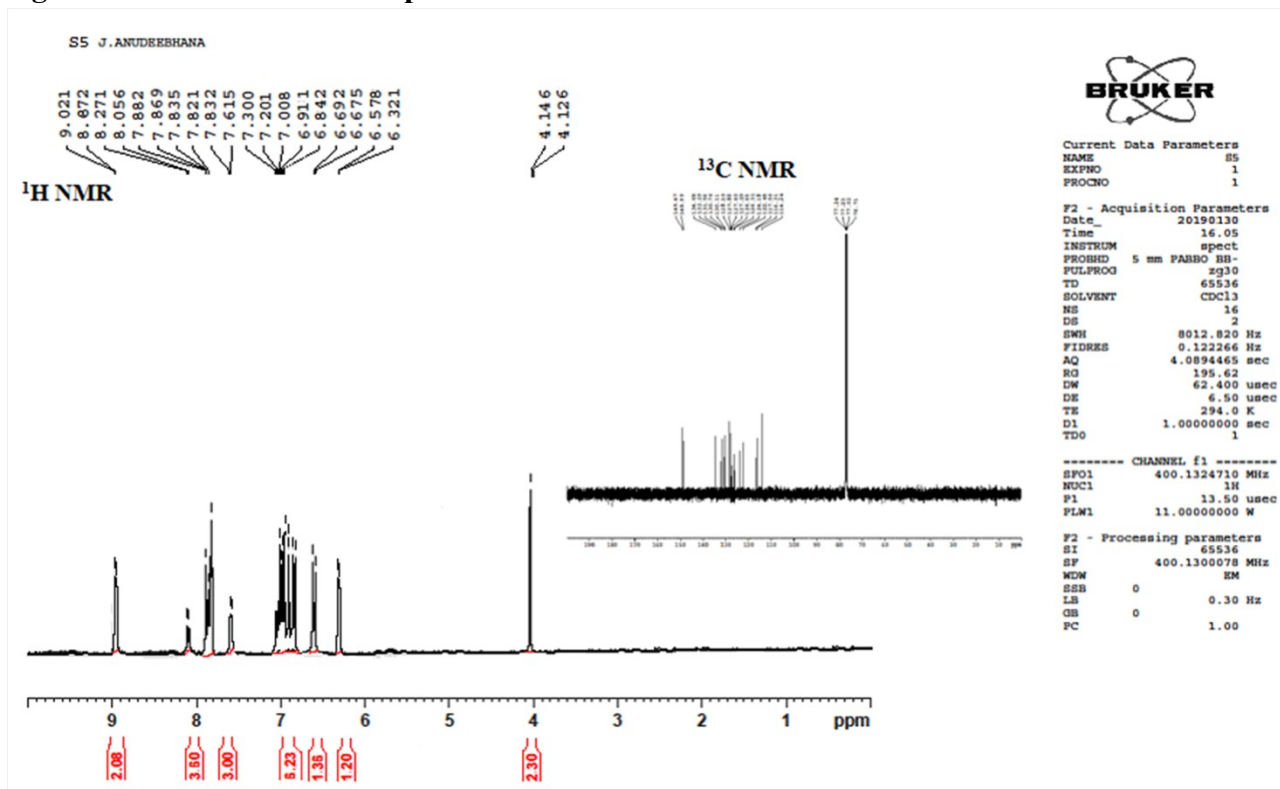
Figure S9. 2 H^1 and C^{13} NMR spectra of *m*-PPI
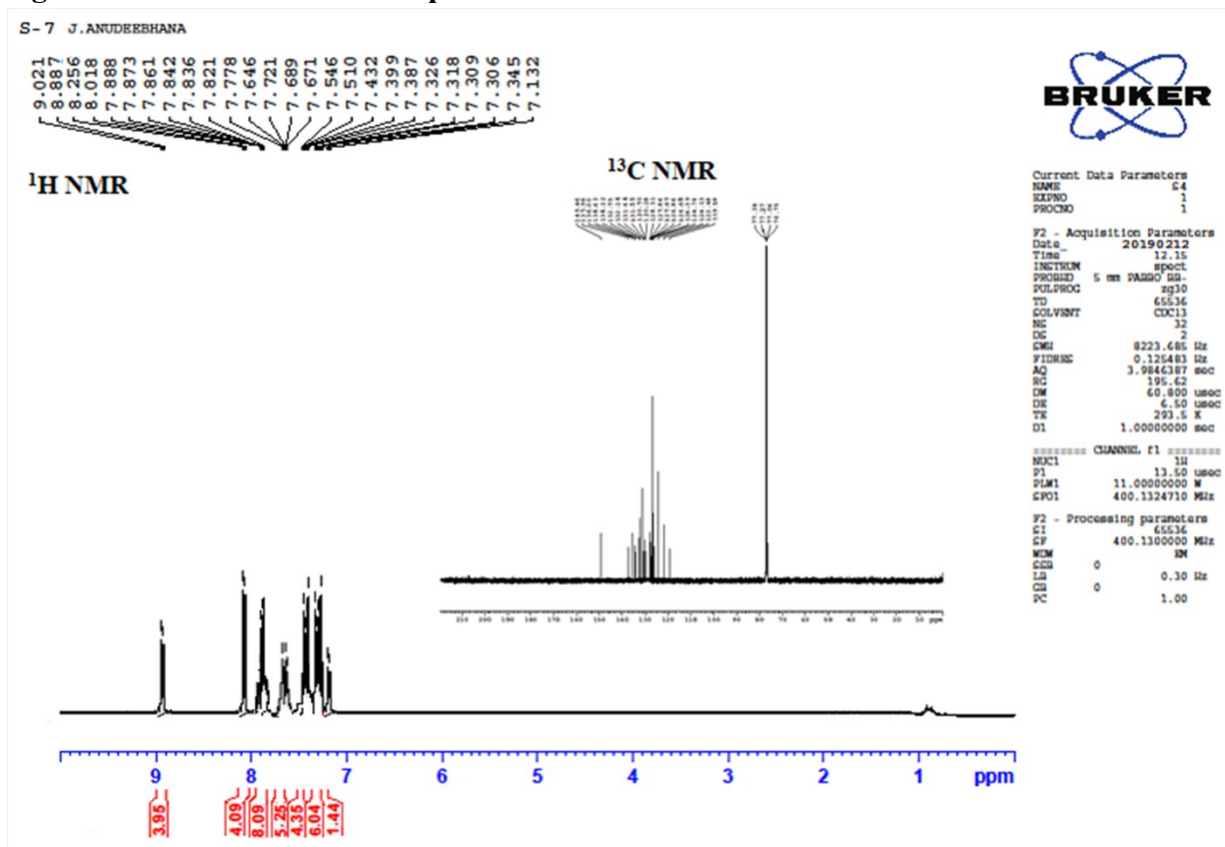
Figure S10 H¹ and C¹³ NMR spectra of *m*-CNNPPI
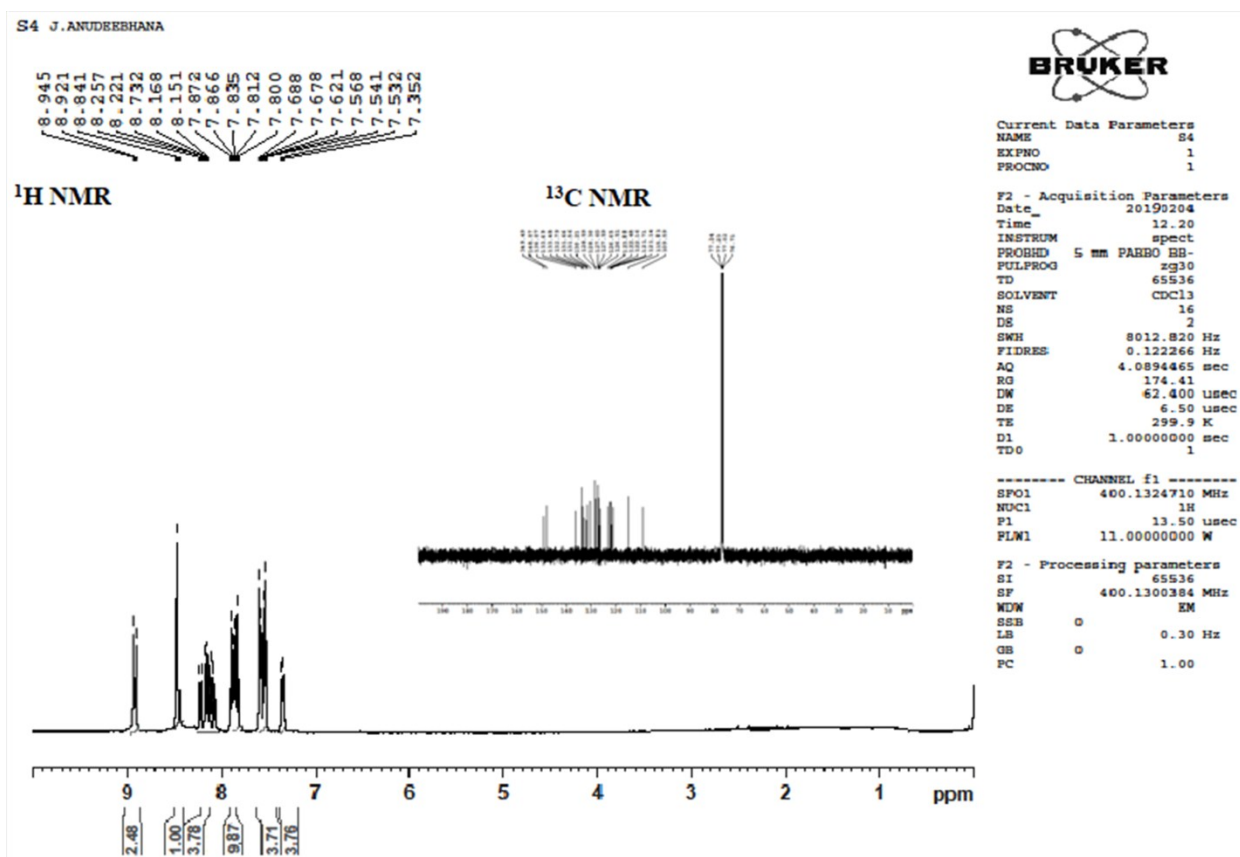
Figure S11. H¹ and C¹³ NMR spectra of *m*-CNAPPI
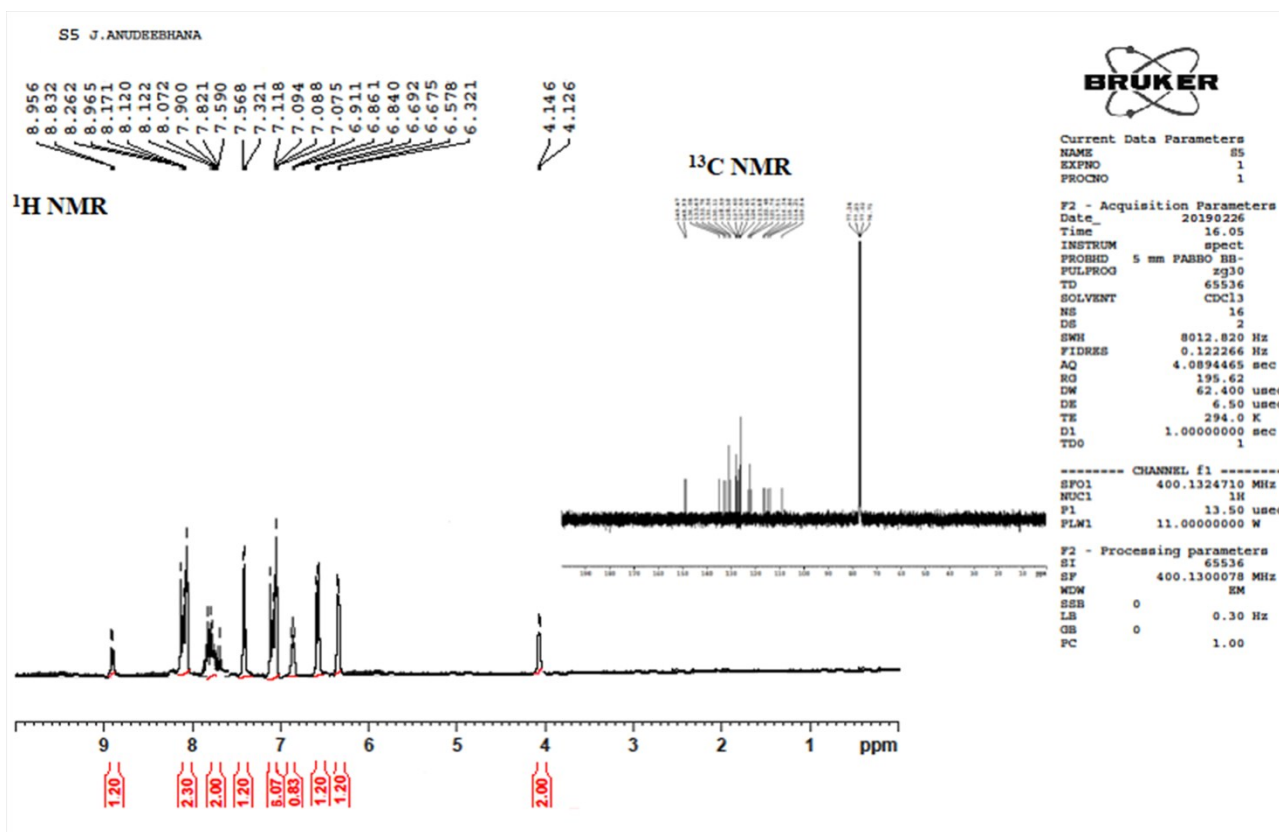
Figure S12. H^1 and C^{13} NMR spectra of *m*-CNPPI
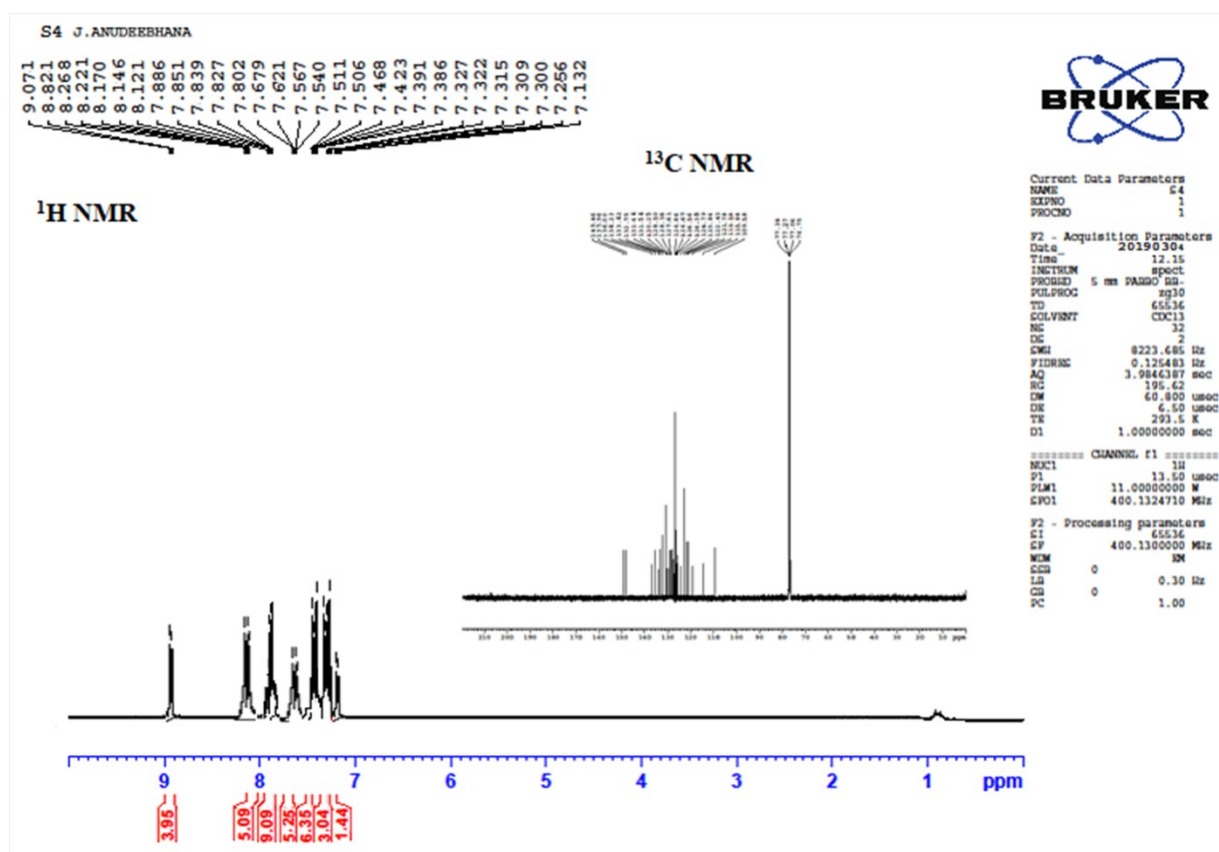
SI–II: Charge-Transfer intexes

The hole-particle pair interactions have been related to the distance covered during the excitations one possible descriptor Δr intex could be used to calculate the average distance which is weighted in function of the excitation coefficients.

$$\Delta r = \frac{\Sigma_{ia} k_{ia}^2 \left| \langle \varphi_a | r | \varphi_a \rangle - \langle \varphi_i | r | \varphi_i \rangle \right|}{\Sigma_{ia} K_{ia}^2}$$

……………….. (S1)

where $\left| \langle \varphi_i | r | \varphi_i \rangle \right|$ is the norm of the orbital centroid [1–4]. Δr–index will be expressed in Å.

The density variation associated to the electronic transition is given by

$$\Delta \rho(r) = \rho_{EX}(r) - \rho_{GS}(r)$$

……………….. (S2)

where $\rho_{GS}(r)$ and $\rho_{EX}(r)$ are the electronic densities of to the ground and excited states, respectively. Two functions, $\rho_+(r)$ and $\rho_-(r)$, corresponds to the points in space where an

increment or a depletion of the density upon absorption is produced and they can be defined as follows:

$$\rho_+(r) = \begin{cases} \Delta\rho(r) & if\ \Delta\rho(r) > 0 \\ 0 & if\ \Delta\rho(r) < 0 \end{cases} \qquad (S3)$$

$$\rho_-(r) = \begin{cases} \Delta\rho(r) & if\ \Delta\rho(r) < 0 \\ 0 & if\ \Delta\rho(r) > 0 \end{cases} \qquad (S4)$$

The barycenters of the spatial regions R_+ and R_- are related with $\rho_+(r)$ and $\rho_-(r)$ and are shown as

$$R_+ = \frac{\int r\rho_+(r)dr}{\int \rho_+(r)dr} = (x_+, y_+, z_+) \qquad (S5)$$

$$R_- = \frac{\int r\rho_-(r)dr}{\int \rho_-(r)dr} = (x_-, y_-, z_-) \qquad (S6)$$

The spatial distance (D_{CT}) between the two barycenters R_+ and R_- of density distributions can thus be used to measure the CT excitation length

$$D_{CT} = |R_+ - R_-| \qquad (S7)$$

The transferred charge (q_{CT}) can be obtained by integrating over all space $\rho_+(\rho_-)$. Variation in dipole moment between the ground and the excited states (μ_{CT}) can be computed by the following relation:

$$\|\mu_{CT}\| = D_{CT}\int \rho_+(r)dr = D_{CT}\int \rho_-(r)dr \qquad (S8)$$

$$= D_{CT}q_{CT} \qquad (S9)$$

The difference between the dipole moments $\|\mu_{CT}\|$ have been computed for the ground and the excited states $\Delta\mu_{ES-GS}$. The two centroids of charges (C^+/C^-) associated to the positive and negative

density regions are calculated as follows. First the root–mean–square deviations along the three axis (σ_{aj}, j = x, y, z; a = + or –) are computed as

$$\sigma_{a,j} = \sqrt{\frac{\sum_i \rho_a(r_i)(j_i - j_a)^2}{\sum_i \rho_a(r_i)}}$$ .... (S10)

The two centroids (C_+ and C_-) are defined as

$$C_+(r) = A_+\, e\left(-\frac{(x-x_+)^2}{2\sigma_{+x}^2} - \frac{(y-y_+)^2}{2\sigma_{+y}^2} - \frac{(z-z_+)^2}{2\sigma_{+z}^2}\right)$$ .... (S11)

$$C_{-+}(r) = A_-\, e\left(-\frac{(x-x_-)^2}{2\sigma_{-x}^2} - \frac{(y-y_-)^2}{2\sigma_{-y}^2} - \frac{(z-z_-)^2}{2\sigma_{-z}^2}\right)$$ .... (S12)

The normalization factors (A+ and A_) are used to impose the integrated charge on the centroid to be equal to the corresponding density change integrated in the whole space:

$$A_+ = \frac{\int \rho_+(r)dr}{\int e\left(-\frac{(x-x_-)^2}{2\sigma_{+x}^2} - \frac{(y-y_-)^2}{2\sigma_{+y}^2} - \frac{(z-z_-)^2}{2\sigma_{+z}^2}\right)dr}$$ .... (S13)

$$A_- = \frac{\int \rho_-(r)dr}{\int e\left(-\frac{(x-x_-)^2}{2\sigma_{-x}^2} - \frac{(y-y_-)^2}{2\sigma_{-y}^2} - \frac{(z-z_-)^2}{2\sigma_{-z}^2}\right)dr}$$ .... (S14)

H index is defined as half of the sum of the centroids axis along the D–A direction, if the D–A direction is along the X axis, H is defined by the relation:

$$H = \frac{\sigma_{+x} + \sigma_{-x}}{2}$$ .... (S15)

The centroid along X axis is expected. The t intex represents the difference between D_{CT} and H:

$$t = D_{CT} - H$$ .... (S16)

14

The integral of hole (h$^+$) and electron (e$^-$) of *p*-PPI, *p*-CNPPI, *m*-PPI and *m*-CNPPI with transition density is displayed in Tables S1-S4. The integral overlap of hole-electron (Figure S20-*p*-PPI; Figure S21- *p*-CNPPI; Figure S22- *m*-PPI; Figure S23- *m*-CNPPI) distribution (S) is a measure of spatial separation of hole and electron. The integral overlap (S) of hole and electron and distance (D) between centroids of hole and electron confirmed the existence of LE and CT states. Compared to parent compounds, the cyano derivatives has high D_{ave} and S_{ave} value, indicates charge transfer is higher in percentage. The variation of dipolemoment with respect to S_0 is outputted which is directly evaluated based on the position of centroid of hole and electron. The RMSD of hole or electron characterizes their distribution breadth: RMSD of both electron and hole in *p*-PPI, *m*-PPI and *m*-CNPPI (Tables S5, S7 & S8) is higher in X direction, indicates electron and hole distribution is much broader in X direction whereas RMSD of hole and electron in *p*-CNPPI (Table S6) is higher in y-direction. The H intex (half sum of the axis of anistropic density variation distribution) measures the spread of positive and negative regions related to CT. The CT intex, *i.e.,* *t* index (D_{CT} - H intex) is another measure of separation of hole-electron (equations S15 and S16; Tables S5- S8). The *t* is negative in all directions which reveal that the overlap of hole and electron is very severe which supports the hybridization. This is further evidenced by Δr intex (equation S1: Tables S9-S12) which is average of hole -electron distance ($d_{h^+ - e^-}$) upon excitation which shows the nature of excitation type, LE or CT: valence excitation (LE) is related to short distance ($< d_{h^+ - e^-}$) while the larger distance ($> d_{h^+ - e^-}$) is related to CT excitation. The triplet exciton is transformed to singlet exciton through RISC process with high energy excited state (hot CT channel) [1] which is beneficial for triplet exciton conversion in electroluminescence process without any delayed fluorescence. The CT excitons are formed with weak binding energy (E_b) on higher excited states, [2] as a result; the exciton utilization (η_s) can be harvested like phosphorescent materials. The enhanced LE component and hybridization between LE and CT components results high η_{PL} and

high η_s. The coexisting LE/CT composition harvested high η_{PL} and high η_s and enhanced OLEDs efficiencies.

Figure S13. Potential energy surface scan (PES) diagram.
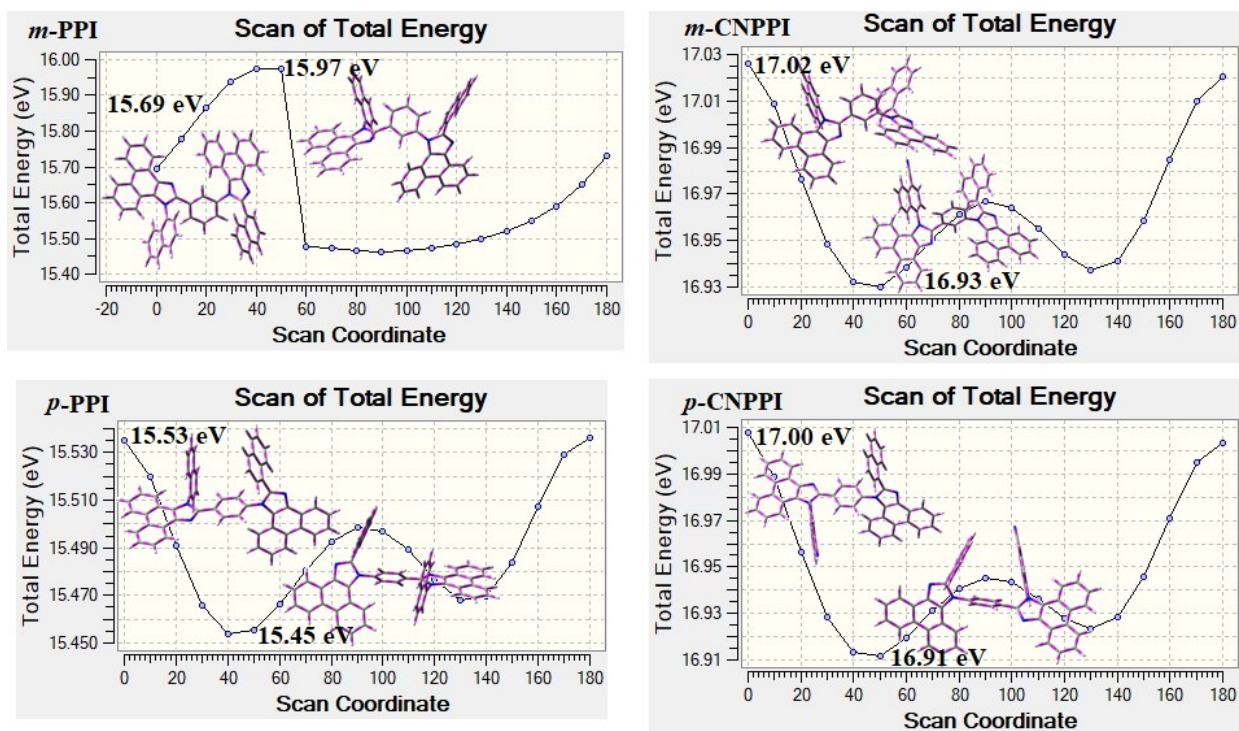
Figure S14. Natural transition orbital pairs (HONTOs and LUNTOs) with transition character for singlet states of *p*-CNPPI [*f*-oscillator strength and % weights of hole-particle].

HONTOs		LUNTOs		HONTOs		LUNTOs
S_1	57 % f-0.5237		S_6	42 % f-0.0358	
S_2	57 % f-0.5237		S_7	29 % f-0.0112	
S_3	62 % f-0.2711		S_8	19 % f-0.0536	
S_4	22 % f-0.0029		S_9	21 % f-0.0730	
S_5	24 % f-0.0461		S_{10}	19 % f-0.0421	

17
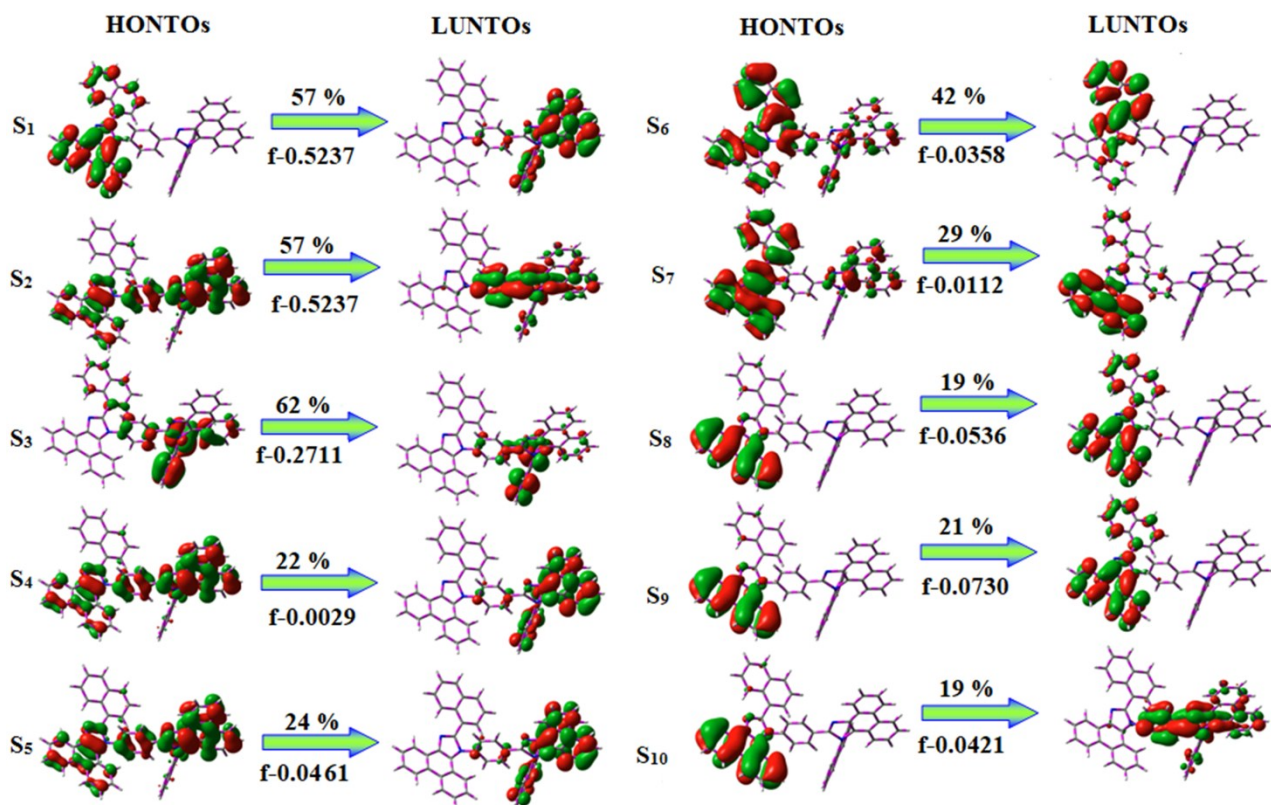
Figure S15. Natural transition orbital pairs(HONTOs and LUNTOs) with transition character for singlet states of *p*-PPI [*f*-oscillator strength and % weights of hole-particle].
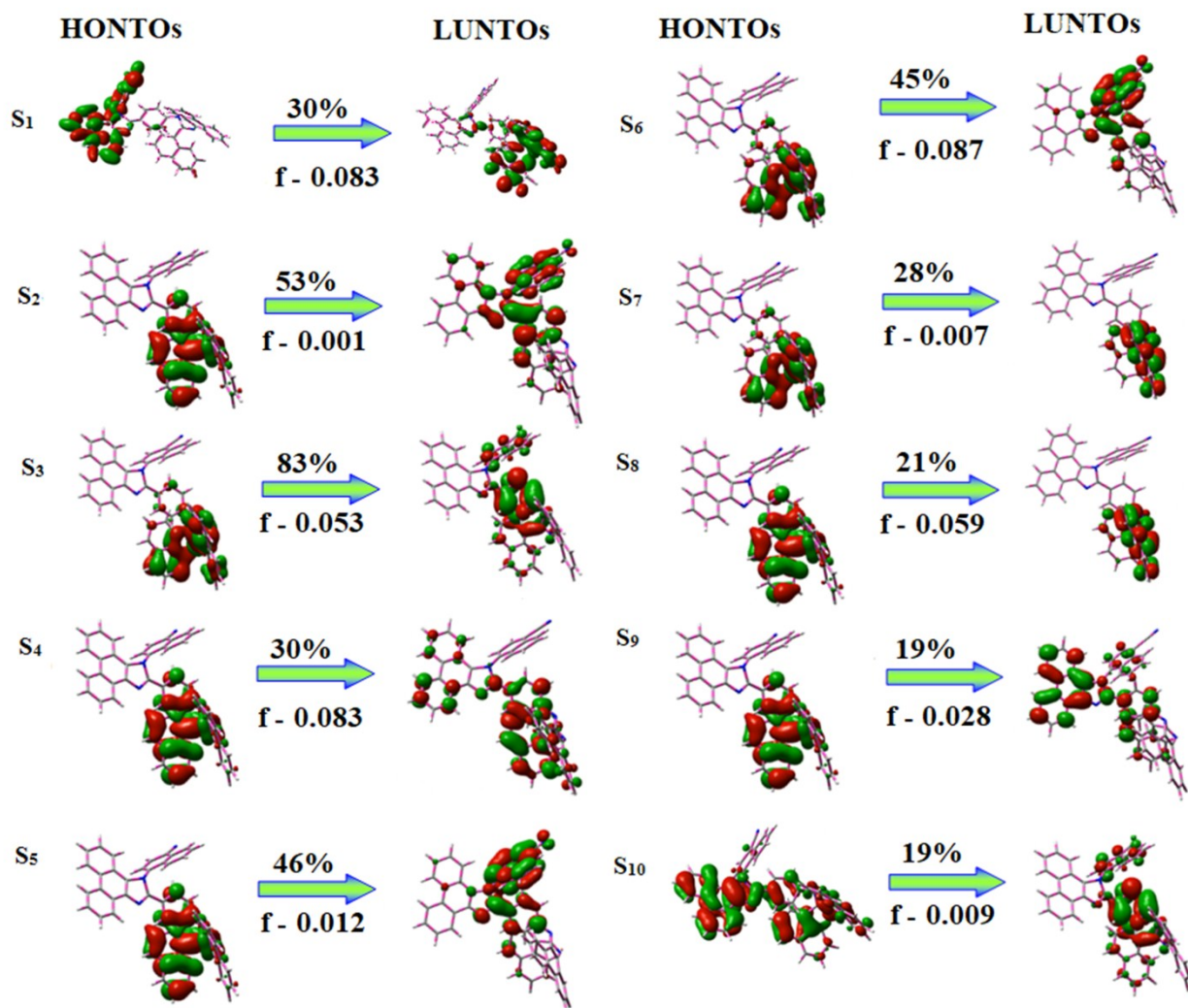
Figure S16. Natural transition orbital pairs (HONTOs & LUNTOs) with transition character for singlet states of *m*-PPI [*f*-oscillator strength and % weights of hole-particle].
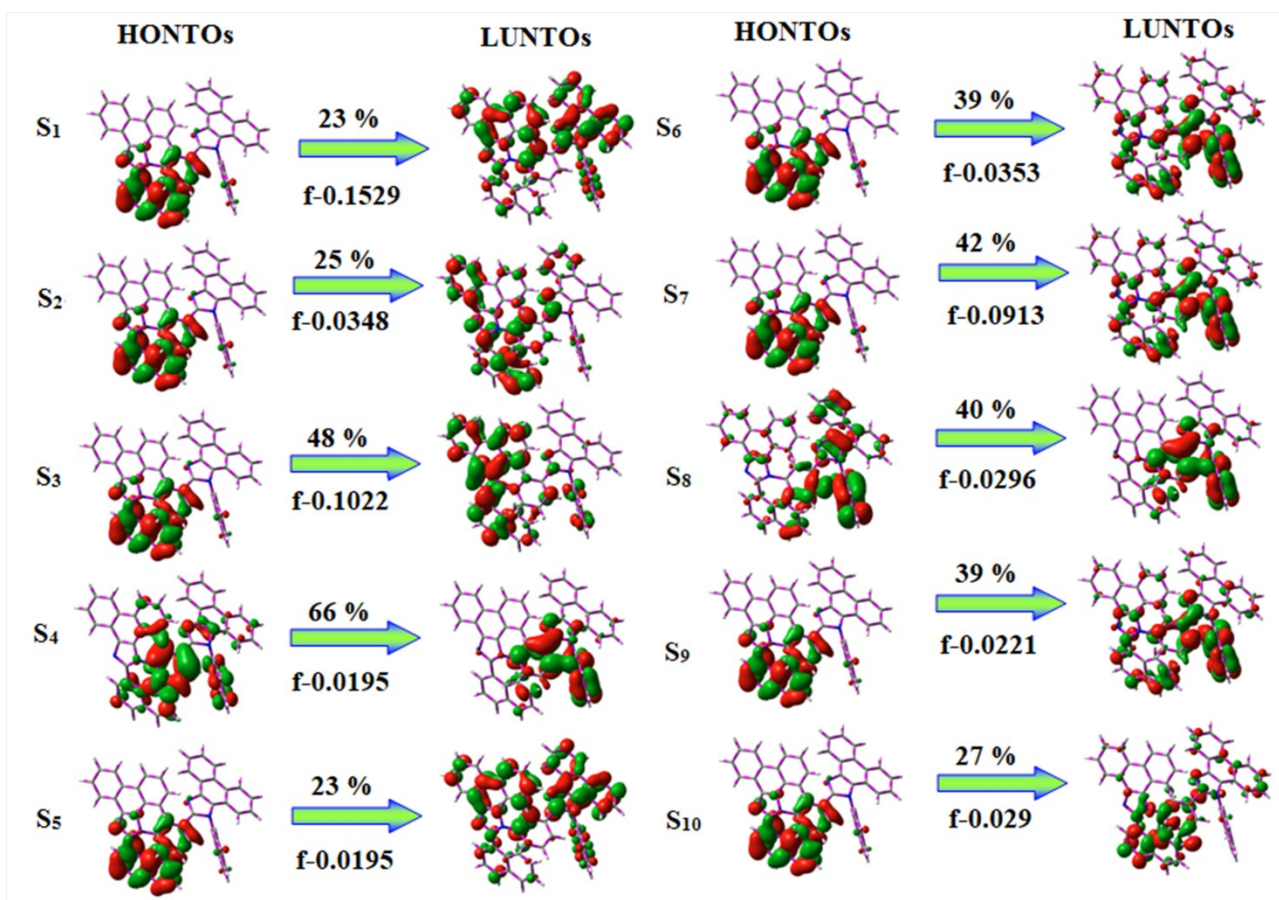
Figure S17. Natural transition orbital pairs (HONTOs & LUNTOs) with transition character for singlet states of *m*-CNPPI [*f*-oscillator strength and % weights of hole-particle].
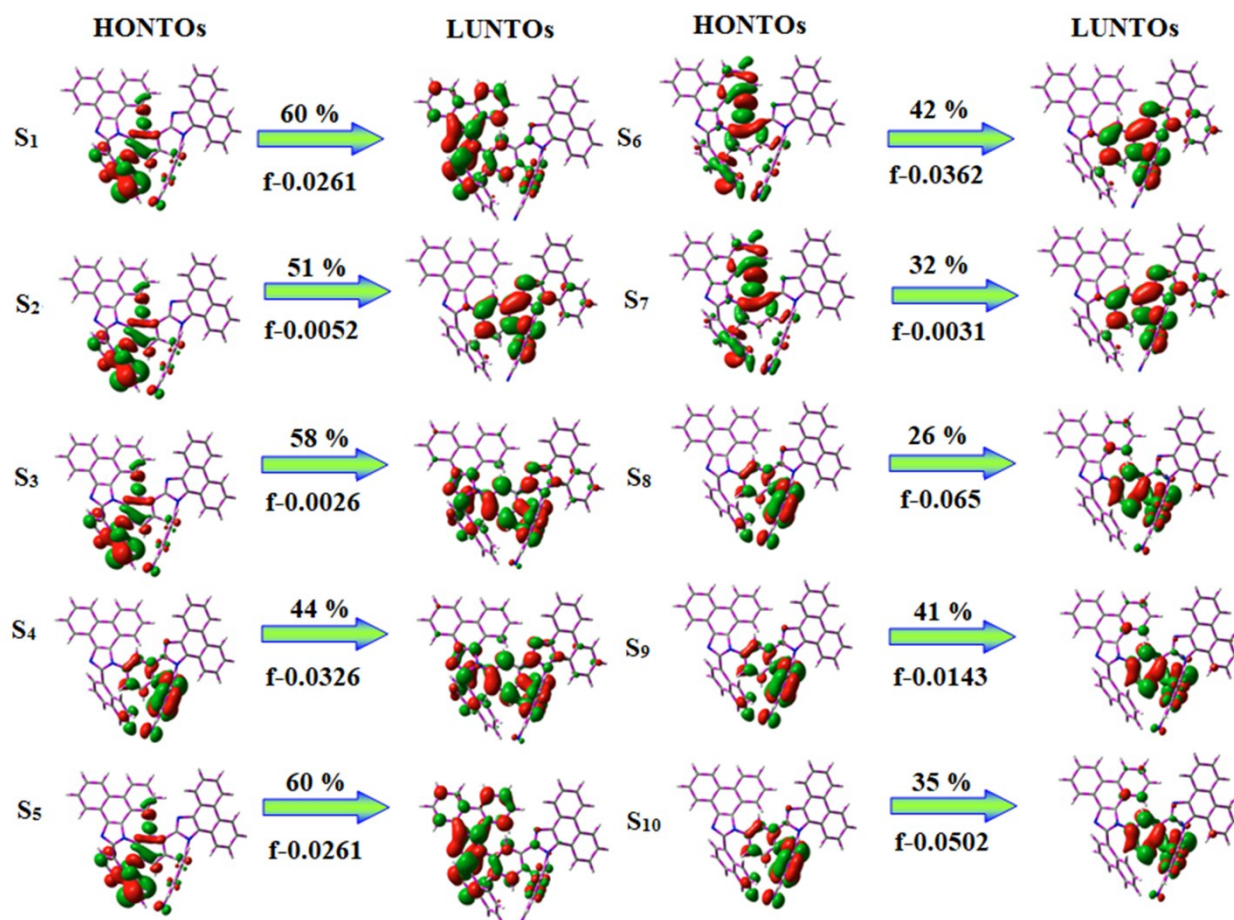
Figure S18. Solvatochromic absorption of (a) *p*-PPI, (b) *p*-CNPPI, (c) *m*-PPI and (d) *m*-CNPPI.
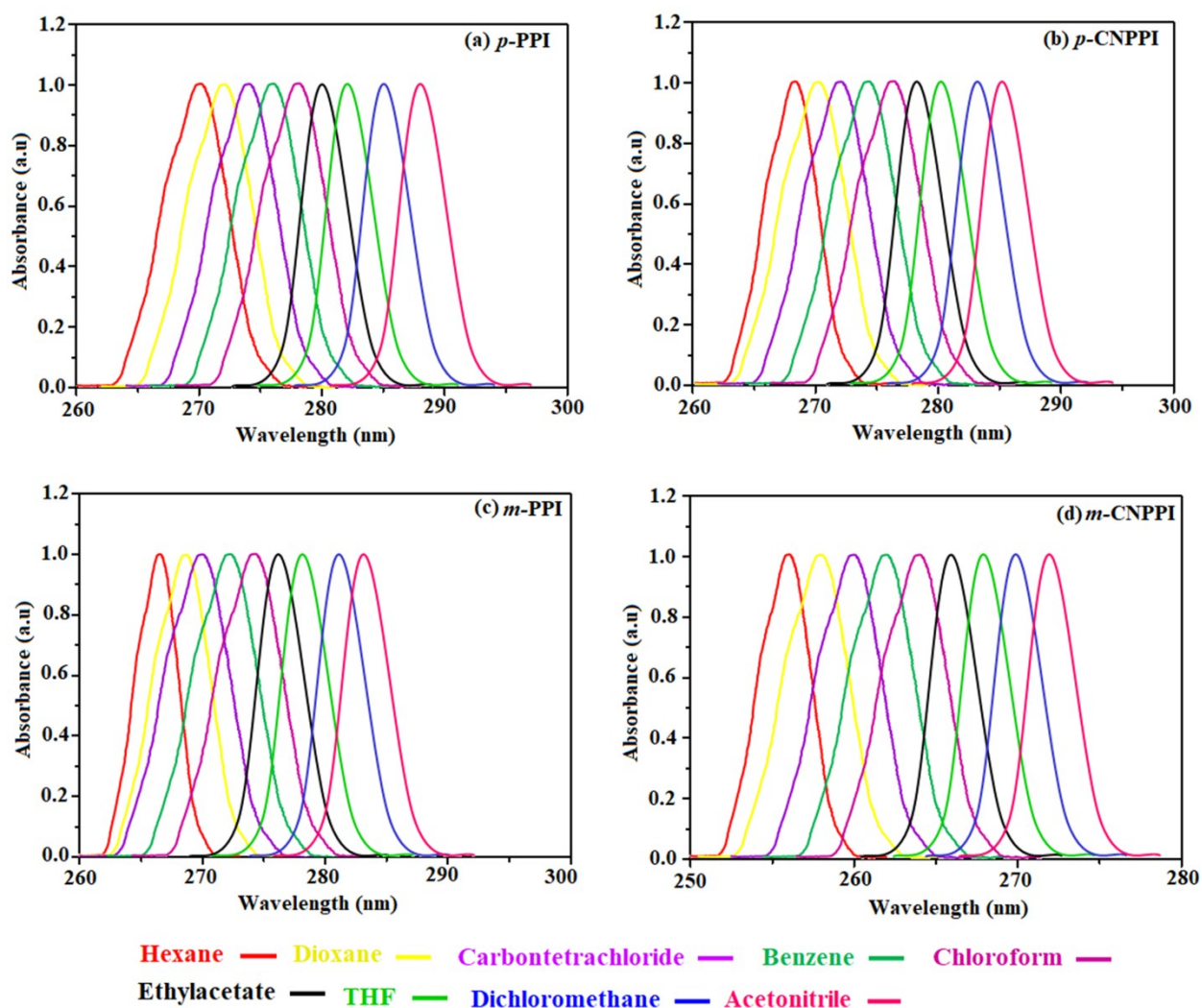
Figure S19. Normalized solvatochromic emission spectra of (a) *p*-PPI, (b) *p*-CNPPI, (c) *m*-PPI and (d) *m*-CNPPI.
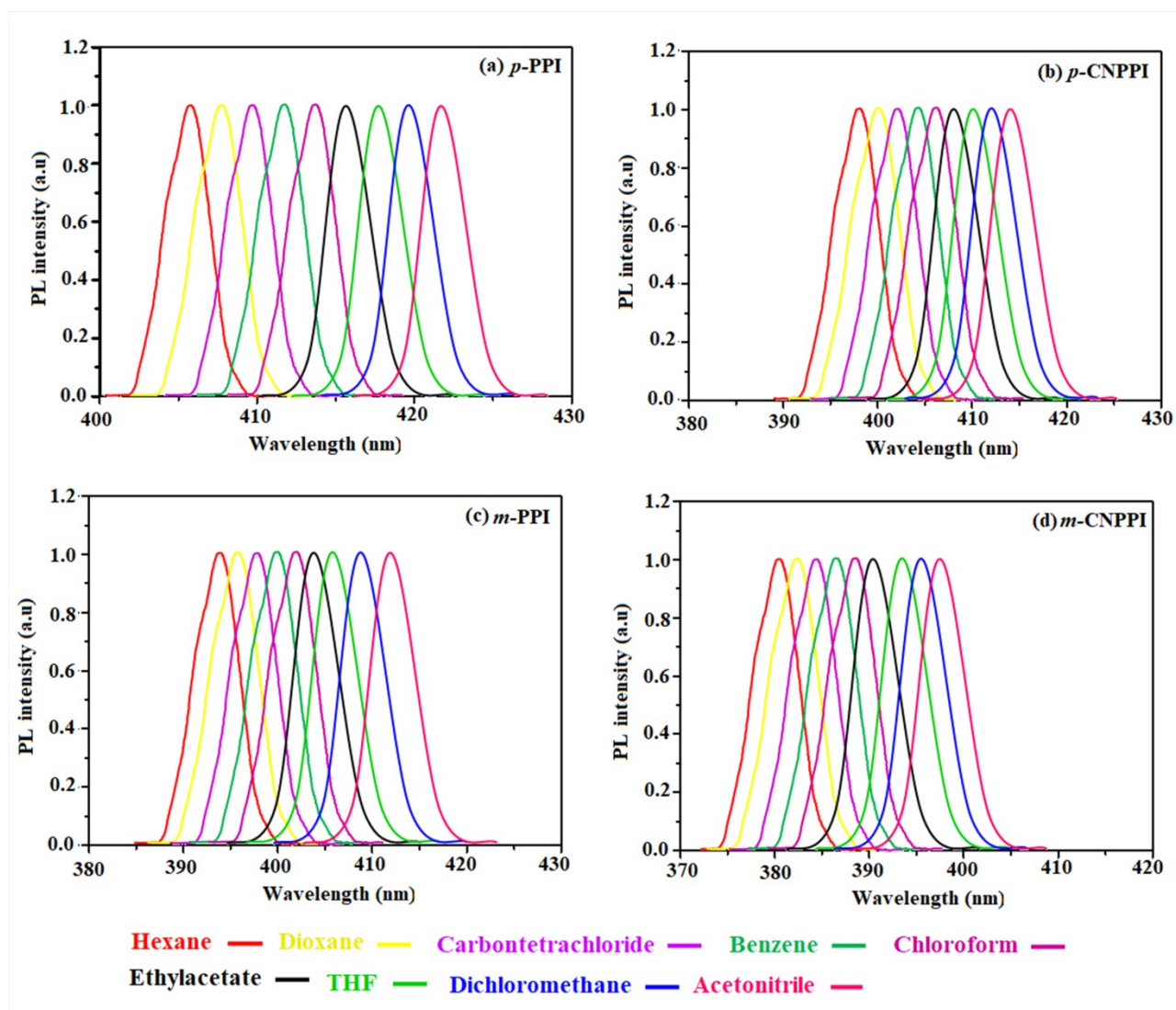
Figure S20. Hole and particle electron density distribution [green increasing and blue decreasing electron density and Transition density matrices (TDM) plot of *p*-PPI.
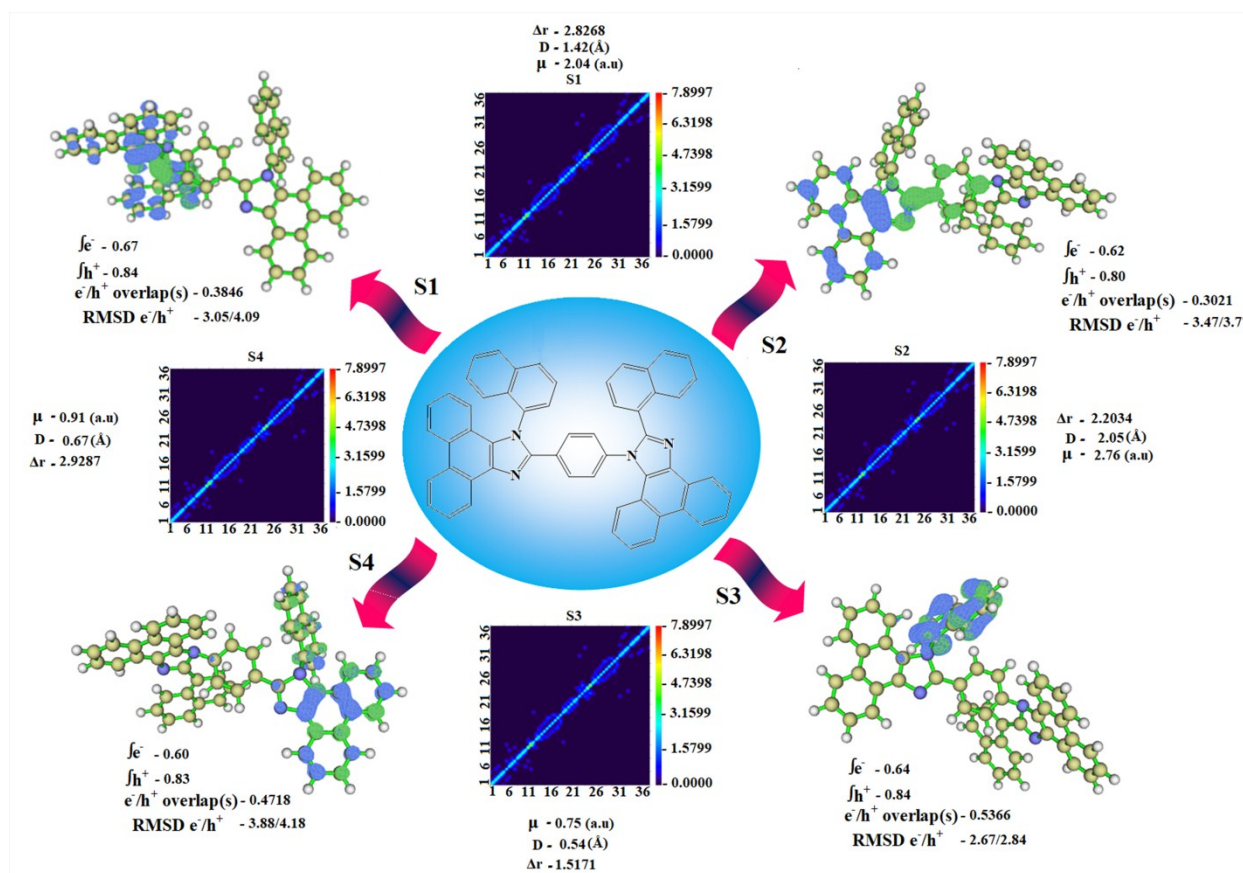
Figure S21. Hole and particle electron density distribution [green increasing and blue decreasing electron density and Transition density matrices (TDM) plot of *p*-CNPPI.
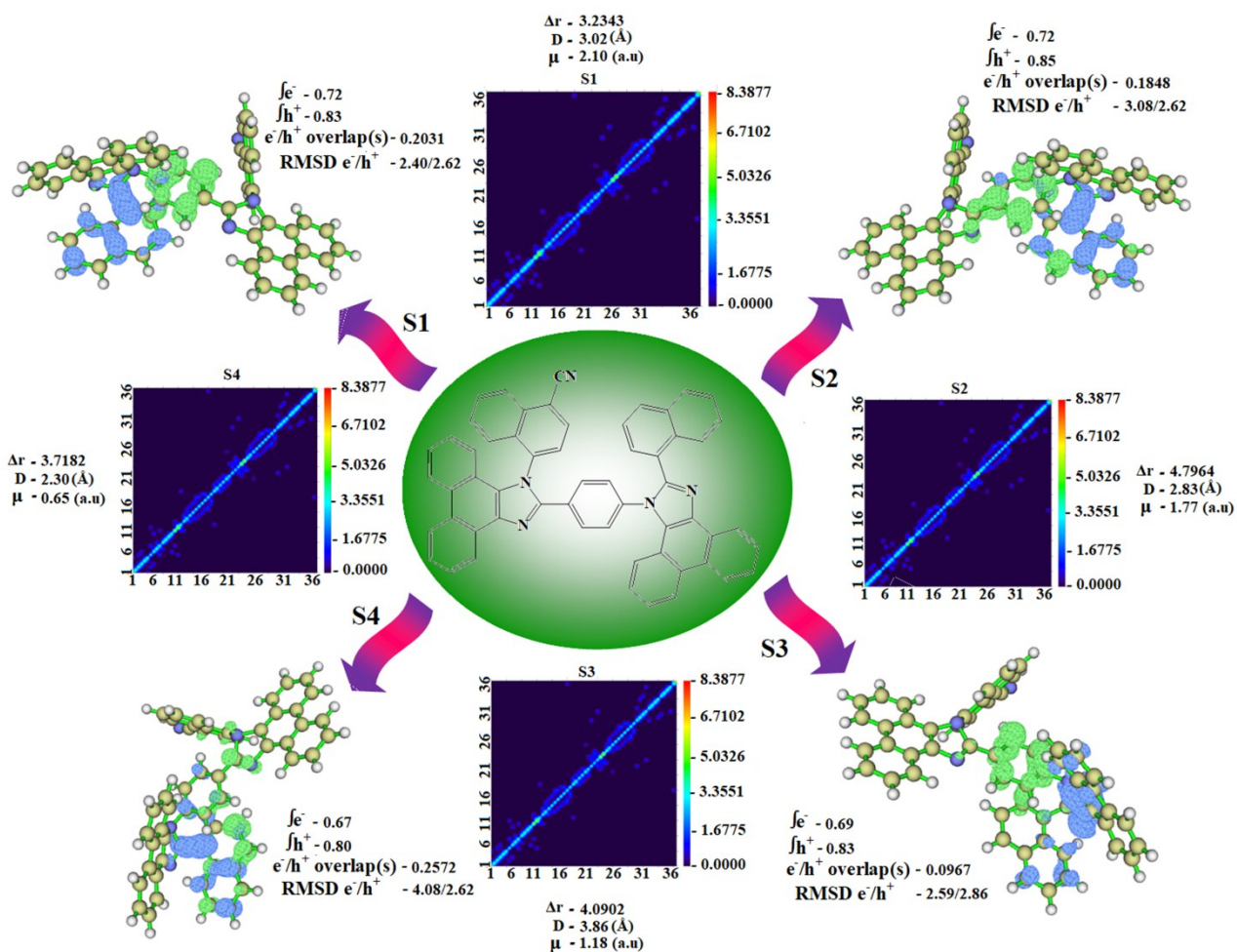
Figure S22. Hole and particle electron density distribution [green increasing and blue decreasing electron density and Transition density matrices (TDM) plot of *m*-PPI.
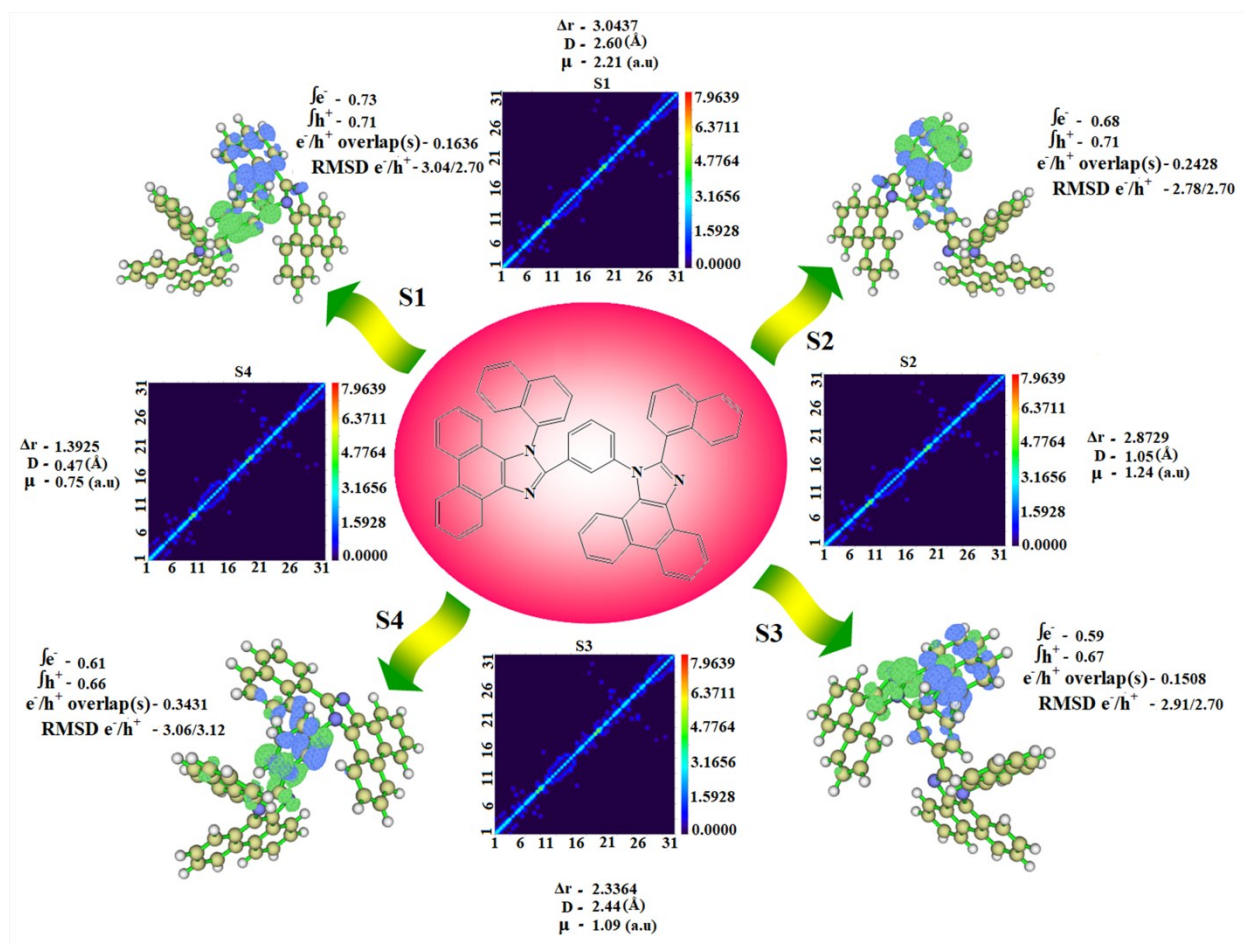
Figure S23. Hole and particle electron density distribution [green increasing and blue decreasing electron density and Transition density matrices (TDM) plot of *m*-CNPPI.
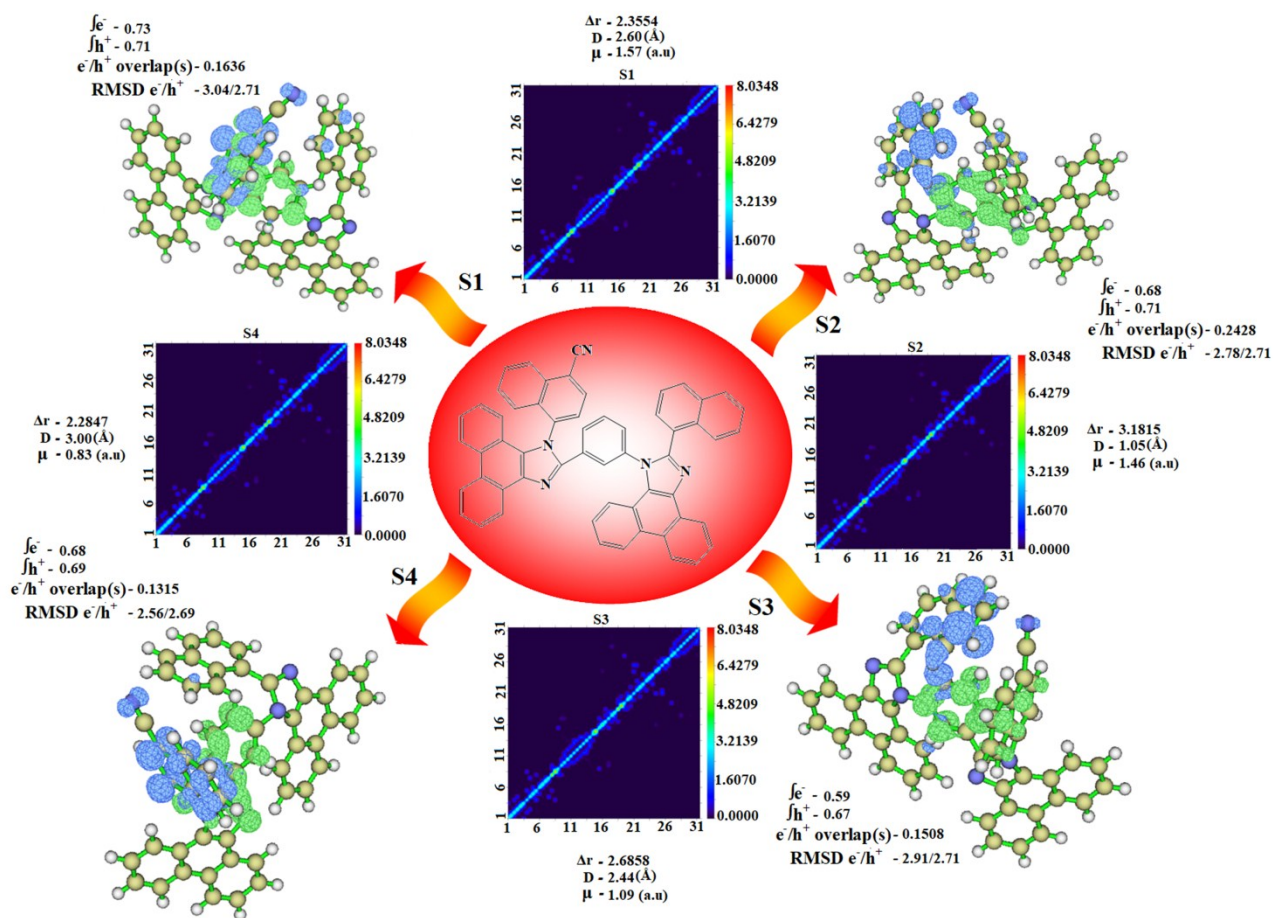
Table S1. Hole and electron overlap (S), distance between centroids of hole and electron (D, Å) and dipole moment (μ) of *p*-PPI.

State	Hole integral	Electron integral	Integral of transition density	Integral overlap of h⁺- e⁻ (S)	Centroid of hole (Å)			Centroid of electron (Å)			D (Å)	μ (a.u)
					x	y	z	x	y	z		
S1	0.8448	0.6681	-0.0138	0.3846	-4.03	0.94	-0.35	-3.37	1.96	-1.10	1.42	2.04
S2	0.8033	0.6193	-0.0104	0.3021	4.32	0.46	1.09	2.35	0.07	0.68	2.05	2.76
S3	0.8418	0.6426	-0.0126	0.5366	3.31	-1.79	-1.89	3.07	-2.19	-2.15	0.54	0.75
S4	0.8316	0.5998	0.0019	0.4718	4.33	-0.01	0.38	4.94	-0.20	0.15	0.67	0.91
S5	0.7754	0.5503	0.0034	0.3893	2.59	-1.15	-1.45	2.94	-1.30	-1.64	0.42	0.53
S6	0.6535	0.4962	-0.0069	0.3060	-3.51	1.41	-0.40	-3.53	2.27	-1.09	1.10	1.19
S7	0.8017	0.5768	0.0007	0.4640	-4.78	-1.26	0.78	-4.86	-1.71	0.98	0.49	0.64
S8	0.7583	0.5411	-0.0049	0.3914	-3.33	2.45	-1.01	-3.34	2.05	-0.93	0.40	0.49
S9	0.5785	0.4430	-0.0002	0.2819	0.29	0.13	0.13	0.15	0.76	0.08	0.64	0.62
S10	0.5717	0.4406	0.0092	0.2319	-0.33	-0.11	-0.55	-0.74	0.73	-0.19	1.01	0.96

Table S2. Hole and electron overlap (S), distance between centroids of hole and electron (D, Å) and dipole moment (μ) of *p*-CNPPI.

State	Hole integral	Electron integral	Integral of transition density	Integral overlap of h⁺- e⁻ (S)	Centroid of hole (Å)			Centroid of electron (Å)			D (Å)	μ (a.u)
					x	y	z	x	y	z		
S1	0.8261	0.7236	-0.0074	0.2031	3.32	-0.12	-1.90	0.84	1.01	-0.60	3.02	4.43
S2	0.8529	0.7231	0.0234	0.1848	3.32	-0.12	-1.90	0.70	-0.04	-0.84	2.83	4.21
S3	0.8260	0.6977	-0.0086	0.0967	4.55	0.32	-0.50	0.75	0.98	-0.60	3.86	5.56
S4	0.8027	0.6706	0.0129	0.2572	3.32	-0.12	-1.90	1.07	-0.14	-1.40	2.30	3.20
S5	0.8750	0.7721	-0.0082	0.0860	3.27	-0.12	-1.93	-2.53	2.77	-0.14	6.73	10.47
S6	0.8475	0.6972	0.0118	0.1176	4.59	0.32	-0.49	0.63	0.01	-0.25	3.98	5.81
S7	0.7715	0.6146	-0.0098	0.2776	4.32	0.19	-0.85	4.25	-0.05	0.73	1.60	2.10
S8	0.6699	0.5298	0.0020	0.2218	3.41	-0.08	-1.50	4.16	0.16	0.54	2.19	2.48
S9	0.7631	0.5848	-0.0082	0.1586	3.21	-0.31	-1.88	-0.66	0.53	-0.13	4.34	5.52
S10	0.7903	0.6017	-0.0006	0.2226	2.8	-0.44	-1.96	0.88	0.84	-0.29	2.85	3.75

Table S3. Hole and electron overlap (S), distance between centroids of hole and electron (D, Å) and dipole moment (μ) of *m*-PPI.

State	Hole integral	Electron integral	Integral of transition density	Integral overlap of h$^+$- e$^-$ (S)	Centroid of hole (Å)			Centroid of electron (Å)			D (Å)	μ (a.u)
					x	y	z	x	y	z		
S1	0.7145	0.7318	-0.0015	0.1636	-1.87	-3.16	-0.66	-0.38	-1.50	0.66	2.60	3.54
S2	0.7061	0.6828	-0.0009	0.2428	-1.87	-3.16	-0.66	-1.60	-3.97	-1.27	1.05	1.37
S3	0.6702	0.5943	-0.0909	0.1508	-1.87	-3.16	-0.66	-3.37	-1.24	-0.49	2.44	2.91
S4	0.6603	0.6071	0.0261	0.3431	-0.28	-1.44	0.71	0.13	-1.28	0.86	0.47	0.56
S5	0.6725	0.6138	-0.0100	0.1090	-1.87	-3.16	-0.66	1.15	-1.35	0.74	3.79	4.61
S6	0.6516	0.6223	-0.0150	0.1068	-1.87	-3.16	-0.66	2.31	-1.99	0.46	4.48	5.39
S7	0.6658	0.5075	0.0390	0.1979	-1.26	-3.01	-0.37	-0.74	-0.99	0.53	2.27	2.52
S8	0.7924	0.6529	-0.0082	0.2940	1.97	-2.51	1.13	1.18	-1.64	0.88	1.20	1.64
S9	0.6298	0.5822	0.0047	0.0856	-1.74	-3.02	-0.55	0.72	-0.97	0.60	3.40	3.90
S10	0.5923	0.4618	-0.0128	0.1547	-1.87	-3.16	-0.66	-0.89	-1.57	-0.21	1.92	1.91

Table S4. Hole and electron overlap (S), distance between centroids of hole and electron (D, Å) and dipole moment (μ) of *m*-CNPPI.

State	Hole integral	Electron integral	Integral of transition density	Integral overlap of h⁺- e⁻ (S)	Centroid of hole (Å)			Centroid of electron (Å)			D (Å)	μ (a.u)
					x	y	z	x	y	z		
S1	0.7145	0.7318	-0.0015	0.1636	-1.87	-3.16	-0.66	-0.38	-1.50	0.66	2.60	3.55
S2	0.7061	0.6828	-0.0009	0.2428	-1.87	-3.16	-0.66	-1.60	-3.97	-1.27	1.05	1.37
S3	0.6701	0.5943	-0.0909	0.1508	-1.87	-3.16	-0.66	-3.37	-1.24	-0.49	2.44	2.91
S4	0.6929	0.6839	-0.0548	0.1315	-1.94	-3.69	-0.30	-3.90	-1.48	-0.78	3.00	3.90
S5	0.5851	0.5941	0.0534	0.1407	-0.80	-0.26	0.29	0.40	-0.50	0.74	1.31	1.46
S6	0.5851	0.5941	0.0534	0.1407	-0.80	-0.26	0.29	0.40	-0.50	0.74	1.31	1.46
S7	0.6456	0.5890	-0.0065	0.1906	-0.02	-1.22	0.45	0.37	-1.38	0.83	0.57	0.66
S8	0.5364	0.4103	0.0765	0.1654	-1.59	-3.04	-0.13	-1.78	-1.97	-0.18	1.08	0.97
S9	0.6138	0.5252	-0.0002	0.1692	0.56	-2.08	0.44	-0.30	-0.71	0.51	1.62	1.74
S10	0.5402	0.5427	0.0350	0.1341	-1.16	-1.15	0.23	-2.22	1.35	-0.15	2.74	2.80

Table S5. Computed RMSD of electron and hole, H index and t index of *p*-PPI.

State	RMSD (Electron)				RMSD (Hole)				H index				t index			
	x	y	z	total	x	y	z	total	x	y	z	Total	x	y	z	Total
S1	1.609	2.302	1.194	3.052	2.199	3.060	1.586	4.089	1.904	2.681	1.390	3.570	-1.249	-1.662	-0.638	2.175
S2	3.029	1.133	1.270	3.475	3.073	1.438	1.645	3.771	3.051	1.285	1.458	3.618	-1.080	-0.900	-1.044	1.751
S3	1.321	1.746	1.530	2.671	1.383	1.777	1.737	2.844	1.352	1.761	1.634	2.757	-1.113	-1.360	-1.371	2.229
S4	2.353	2.085	2.280	3.883	3.045	1.892	2.146	4.178	2.699	1.988	2.213	4.017	-2.096	-1.799	-1.981	3.399
S5	2.702	2.483	1.830	4.101	3.033	2.383	1.936	4.315	2.867	2.433	1.883	4.206	-2.517	-2.285	-1.699	3.800
S6	1.779	2.515	1.314	3.349	2.645	2.978	1.531	4.267	2.212	2.747	1.423	3.803	-2.201	-1.891	-0.735	2.994
S7	2.376	2.118	1.228	3.411	2.704	2.130	1.335	3.692	2.540	2.124	1.282	3.550	-2.460	-1.678	-1.081	3.168
S8	2.388	2.745	1.490	3.931	2.426	2.788	1.421	3.960	2.407	2.766	1.455	3.945	-2.393	-2.375	-1.373	3.640
S9	4.676	2.243	1.845	5.505	5.030	2.241	1.815	5.799	4.853	2.242	1.830	5.651	-4.716	-1.615	-1.778	5.292
S10	4.034	2.200	1.644	4.881	4.575	2.473	1.803	5.505	4.305	2.336	1.724	5.192	-3.889	-1.493	-1.358	4.381

Table S6. Computed RMSD of electron and hole, H index and t index of *p*-CNPPI.

State	RMSD (Electron)				RMSD (Hole)				H index				t index			
	x	y	z	total	x	y	z	total	x	y	z	Total	x	y	z	Total
S1	1.742	1.236	1.095	2.400	1.687	1.334	1.501	2.623	1.714	1.285	1.298	2.505	0.770	-0.154	0.002	0.785
S2	2.240	1.561	1.431	3.083	1.687	1.334	1.501	2.623	1.964	1.448	1.466	2.846	0.656	-1.367	-0.404	1.569
S3	1.935	1.301	1.132	2.592	1.425	1.261	2.135	2.860	1.680	1.281	1.633	2.671	2.122	-0.624	-1.534	2.691
S4	3.149	1.926	1.750	4.085	1.687	1.334	1.501	2.623	2.418	1.630	1.625	3.339	-0.171	-1.612	-1.123	1.972
S5	2.231	2.038	1.724	3.480	1.704	1.345	1.454	2.613	1.968	1.692	1.589	3.043	3.835	1.206	0.204	4.025
S6	2.620	1.442	1.493	3.343	1.352	1.245	2.153	2.831	1.986	1.343	1.823	3.012	1.980	-1.037	-1.580	2.737
S7	2.958	1.239	1.936	3.746	1.450	1.256	2.130	2.866	2.204	1.247	2.033	3.247	-2.137	-1.007	-0.448	2.405
S8	2.960	1.354	1.879	3.758	2.017	1.358	1.807	3.030	2.488	1.356	1.843	3.380	-1.748	-1.113	0.205	2.083
S9	3.020	1.786	1.167	3.698	1.944	1.365	1.621	2.876	2.482	1.576	1.394	3.254	1.392	-0.728	0.363	1.612
S10	2.659	1.535	1.529	3.430	2.414	1.348	1.547	3.168	2.537	1.442	1.538	3.298	-0.622	-0.156	0.139	0.656

Table S7. Computed RMSD of electron and hole, H index and t index of *m*-PPI.

State	RMSD (Electron)				RMSD (Hole)				H index				t index			
	x	y	z	total	x	y	z	total	x	y	z	Total	x	y	z	Total
S1	2.056	1.887	1.217	3.044	1.566	1.480	1.640	2.707	1.811	1.683	1.428	2.855	-0.317	-0.022	-0.103	0.334
S2	1.673	1.545	1.600	2.784	1.566	1.480	1.640	2.707	1.619	1.512	1.620	2.745	-1.354	-0.697	-1.019	1.833
S3	1.588	1.920	1.508	2.912	1.566	1.480	1.640	2.707	1.577	1.700	1.574	2.802	-0.080	0.217	-1.404	1.423
S4	2.168	1.861	1.110	3.065	2.167	1.859	1.257	3.120	2.168	1.860	1.184	3.092	-1.752	-1.698	-1.037	2.652
S5	2.736	2.133	1.428	3.752	1.566	1.480	1.640	2.707	2.151	1.806	1.534	3.200	0.867	0.004	-0.123	0.876
S6	2.482	2.004	1.549	3.546	1.566	1.480	1.640	2.707	2.024	1.742	1.595	3.110	2.156	-0.577	-0.470	2.280
S7	3.380	2.619	1.621	4.573	2.244	1.611	1.753	3.272	2.812	2.115	1.687	3.902	-2.294	-0.092	-0.789	2.427
S8	2.444	1.923	1.357	3.393	2.211	1.621	1.517	3.134	2.328	1.772	1.437	3.259	-1.538	-0.904	-1.184	2.141
S9	3.809	2.604	1.743	4.933	1.666	1.586	1.650	2.831	2.738	2.095	1.697	3.842	-0.277	-0.044	-0.544	0.612
S10	3.202	2.584	1.981	4.566	1.566	1.480	1.640	2.707	2.384	2.032	1.810	3.618	-1.408	-0.443	-1.359	2.007

Table S8. Computed RMSD of electron and hole, H index and t index of *m*-CNPPI.

State	RMSD (Electron)				RMSD (Hole)				H index				t index			
	x	y	z	total	x	y	z	total	x	y	z	Total	x	y	z	Total
S1	2.056	1.887	1.217	3.044	1.566	1.480	1.640	2.707	1.811	1.683	1.428	2.855	-0.317	-0.022	-0.103	0.334
S2	1.673	1.545	1.600	2.784	1.566	1.480	1.640	2.707	1.619	1.512	1.620	2.745	-1.354	-0.697	-1.019	1.833
S3	1.588	1.920	1.508	2.912	1.566	1.480	1.640	2.707	1.577	1.700	1.574	2.802	-0.080	0.217	-1.404	1.423
S4	1.212	1.796	1.355	2.556	1.299	1.973	1.289	2.691	1.256	1.885	1.322	2.622	0.706	0.330	-0.836	1.143
S5	1.947	1.907	0.992	2.900	1.528	2.985	1.032	3.509	1.738	2.446	1.012	3.166	-0.533	-2.208	-0.561	2.340
S6	1.947	1.907	0.992	2.900	1.528	2.985	1.032	3.509	1.738	2.446	1.012	3.166	-0.533	-2.208	-0.561	2.340
S7	1.737	1.619	1.116	2.624	1.925	2.823	1.372	3.682	1.831	2.221	1.244	3.136	-1.441	-2.054	-0.866	2.655
S8	2.306	2.833	1.313	3.881	1.535	2.553	1.288	3.245	1.920	2.693	1.300	3.554	-1.738	-1.629	-1.249	2.689
S9	2.091	2.316	0.985	3.272	1.834	2.671	1.412	3.534	1.963	2.493	1.199	3.392	-1.105	-1.123	-1.127	1.937
S10	2.369	3.451	1.077	4.322	1.414	3.152	1.059	3.613	1.891	3.301	1.068	3.951	-0.839	-0.802	-0.685	1.347

.

Table S9. Excitation energy (eV), excitation coefficient and Δr intex (Å) of *p*-PPI.

State	Singlet			Triplet		
	Excitation energy	Excitation coefficient	Δr intex	Excitation energy	Excitation coefficient	Δr intex
1	3.2703	0.4088	2.8168	1.2421	0.7347	2.1928
2	3.3933	0.3913	2.2034	1.6382	0.6005	2.6795
3	3.5708	0.4028	1.5171	1.7574	0.7137	3.6964
4	3.6164	0.3903	2.9287	1.8267	0.4700	1.6542
5	3.6407	0.3612	2.1019	1.8621	0.6741	2.8306
6	3.6515	0.3033	1.6490	1.9642	0.7257	2.5651
7	3.7464	0.3769	3.2094	2.2518	0.6418	2.4273
8	3.7835	0.3469	2.3971	2.2738	0.6366	4.8961
9	3.9408	0.2839	2.4267	2.3567	0.4896	3.3768
10	3.9538	0.2803	2.3975	2.4910	0.4527	2.8496

Table S10. Excitation energy (eV), excitation coefficient and Δr intex (Å) of *p*-CNPPI.

State	Singlet		
	Excitation energy	**Excitation coefficient**	**Δr intex**
1	0.7975	0.4564	3.2343
2	1.1326	0.4712	4.7964
3	1.7248	0.4396	4.0902
4	2.2512	0.4435	3.7182
5	2.3754	0.4840	4.6199
6	2.4168	0.4506	5.4468
7	2.5755	0.4138	2.8682
8	2.7131	0.3586	2.6000
9	2.8425	0.4094	4.1256
10	2.9032	0.3935	3.4087

Table S11. Excitation energy (eV), excitation coefficient and Δr intex (Å) of *m*-PPI.

State	Singlet		
	Excitation energy	Excitation coefficient	Δr intex
1	0.5997	0.4666	3.0437
2	1.5712	0.4612	2.8729
3	1.7273	0.4377	2.3364
4	2.0665	0.3821	1.3925
5	2.0757	0.4393	3.0422
6	2.1701	0.4256	2.8190
7	2.5535	0.4200	2.7773
8	2.6330	0.4106	2.1899
9	2.8093	0.4075	3.4323
10	2.8155	0.3869	2.8880

Table S12. Excitation energy (eV), excitation coefficient and Δr intex (Å) of *m*-CNPPI.

State	Singlet			Triplet		
	Excitation energy	Excitation coefficient	Δr intex	Excitation energy	Excitation coefficient	Δr intex
1	0.4743	0.4646	2.3554	1.2118	0.8521	0.7524
2	0.5846	0.4470	3.1815	1.3637	0.8232	2.5474
3	0.9489	0.4489	2.6858	1.4339	0.7384	2.5612
4	1.2134	0.4443	2.2847	1.5224	0.7294	2.0407
5	1.4712	0.4369	3.2150	1.6485	0.7938	2.1733
6	1.5469	0.3997	1.8758	1.7580	0.70350	2.1163
7	1.8385	0.4224	1.8674	1.8139	0.6601	2.0937
8	1.9125	0.3442	2.4355	1.8240	0.6540	1.8880
9	1.9501	0.3918	1.9242	1.8616	0.7903	2.5198
10	2.0421	0.3690	2.7169	2.1267	0.6669	1.9693

Table S13. Singlet (E_S) energies (eV), oscillator strength (f), dipole moment (μ, D) of p-CNPPI.

Energy level	E_S	Oscillator strength (f)	μ	NTO Transitions
1	0.8	0.07	2.11	85% $143 \rightarrow 144$
2	1.13	0.01	1.77	53% $143 \rightarrow 146$
3	1.72	0.05	1.18	83% $142 \rightarrow 144$
4	2.25	0.08	0.65	30% $143 \rightarrow 154$
5	2.38	0.01	0.53	46% $143 \rightarrow 145$
6	2.42	0.09	0.49	45% $142 \rightarrow 146$
7	2.58	0.01	0.33	28% $142 \rightarrow 150$
8	2.71	0.06	0.19	21% $143 \rightarrow 150$
9	2.84	0.03	0.06	19% $143 \rightarrow 147$
10	2.9	0.01	0.00	19% $140 \rightarrow 144$

Table S14. Computed singlet (E_S) and triplet (E_T) energies (eV), oscillator strength (f), dipole moment (μ, D) and singlet-triplet splitting (ΔE_{ST}, eV) of *p*-PPI.

Energy level	E_S	Oscillator strength (f)	μ	NTO Transitions	E_T	ΔE_{ST}	NTO Transitions
1	3.27	0.46	2.04	59% $138 \rightarrow 140$	1.24	2.26	57% $137 \rightarrow 141$
2	3.39	0.52	2.76	57% $139 \rightarrow 142$	1.64	2.52	30% $138 \rightarrow 141$
3	3.57	0.27	0.75	62% $137 \rightarrow 141$	1.76	2.67	28% $139 \rightarrow 142$
4	3.62	0.01	0.91	22% $139 \rightarrow 144$	1.83	2.73	18% $134 \rightarrow 142$
5	3.64	0.05	0.53	24% $139 \rightarrow 144$	1.86	2.75	26% $140 \rightarrow 147$
6	3.65	0.04	1.19	42% $136 \rightarrow 140$	1.96	2.81	54% $140 \rightarrow 150$
7	3.75	0.01	0.64	29% $138 \rightarrow 146$	2.25	3.00	31% $137 \rightarrow 153$
8	3.78	0.05	0.49	19% $134 \rightarrow 143$	2.27	3.03	32% $137 \rightarrow 139$
9	3.94	0.07	0.62	21% $134 \rightarrow 143$	2.36	3.15	20% $137 \rightarrow 152$
10	3.95	0.04	0.96	19% $137 \rightarrow 142$	2.49	3.22	20% $136 \rightarrow 139$

Table S15. Computed singlet (E_S) and triplet (E_T) energies (eV), oscillator strength (*f*), dipole moment (μ, D) and singlet-triplet splitting (ΔE_{ST}, eV) of *m*-CNPPI.

Energy level	E_S	Oscillator strength (*f*)	μ	NTO Transitions	E_T	ΔE_{ST}	NTO Transitions
1	0.47	0.01	1.5678	52% $142 \rightarrow 144$	1.11	0.79	92% $141 \rightarrow 143$
2	0.58	0.01	1.4575	51% $143 \rightarrow 144$	1.36	0.97	85% $142 \rightarrow 143$
3	0.95	0.00	1.0932	58% $143 \rightarrow 145$	1.43	1.19	43% $142 \rightarrow 145$
4	1.21	0.03	0.8287	44% $142 \rightarrow 145$	1.52	1.36	51% $141 \rightarrow 146$
5	1.47	0.03	0.5709	60% $143 \rightarrow 146$	1.65	1.56	50% $142 \rightarrow 150$
6	1.55	0.04	0.4952	42% $141 \rightarrow 144$	1.76	1.65	46% $143 \rightarrow 150$
7	1.84	0.00	0.2036	32% $141 \rightarrow 144$	1.81	1.82	29% $140 \rightarrow 143$
8	1.91	0.07	0.1296	26% $142 \rightarrow 151$	1.82	1.86	24% $140 \rightarrow 145$
9	1.95	0.01	0.0920	41% $142 \rightarrow 151$	1.86	1.90	43% $141 \rightarrow 144$
10	2.04	0.05	0.0000	35% $142 \rightarrow 151$	2.13	2.08	30% $142 \rightarrow 143$

Table S16. Computed singlet (E_S) and triplet (E_T) energies (eV), oscillator strength (f), dipole moment (μ, D) of *m*-PPI.

Energy level	E_S	Oscillator strength (f)	μ	NTO Transition
1	0.6	0.01	2.22	71% $139 \rightarrow 140$
2	1.57	0.03	1.24	25% $139 \rightarrow 149$
3	1.73	0.10	1.09	48% $139 \rightarrow 142$
4	2.07	0.15	0.75	66% $138 \rightarrow 140$
5	2.08	0.02	0.74	23% $139 \rightarrow 143$
6	2.17	0.04	0.65	39% $139 \rightarrow 141$
7	2.55	0.09	0.26	42% $139 \rightarrow 141$
8	2.63	0.03	0.18	40% $135 \rightarrow 140$
9	2.81	0.02	0.01	39% $139 \rightarrow 141$
10	2.82	0.03	0.00	27% $139 \rightarrow 156$

Reference

[1] (a) M. Segal, M. Singh, K. Rivoir, S. Difley, T. V. Voorhis, M. A. Baldo, *Nat. Mater.,* **2007**, 6, 374; (b) W. Barford, *Phys. Rev. B.,* **2004**, 70, 205204.

[2] W. Jiang, L. Duan Qiao, *J. Org. Lett.,* **2011**, 13, 3146.